# DEVELOPMENT OF A HUMAN BODY MODEL (THUMS VERSION 7) TO SIMULATE KINEMATICS AND INJURIES OF RECLINED OCCUPANTS IN FRONTAL COLLISIONS

**Takao Matsuda**
**Naoya Kobayashi**
**Noriyuki Fujita**
**Yuichi Kitagawa**
Toyota Motor Corporation
Japan

Paper Number 23-0030

## ABSTRACT

This paper describes the development of THUMS Version 7 which is a virtual human body model (HBM) to be used for simulating impact kinematics and injuries of occupants assuming a reclined seating posture in vehicle frontal collisions. In highly automated vehicles, it is expected that occupants wish to take various sitting positions including a reclined posture. Prior research has found that there is a relatively high possibility of injury to the occupant for a reclined posture in vehicle collisions. If the lap belt engagement with the pelvis is lost in a frontal collision, there is the possibility that the internal organs are highly loaded. The latest released Version 6 does not have precise representation of the small intestine but has a generic soft solid. It was decided to upgrade THUMS for accurate prediction of internal organ injury. The geometry and mechanical properties of the small intestine and the other relevant body parts were fundamentally revised in Version 7. The interaction between the pelvis and lap belt was most important in simulating occupant kinematics leading to the abdominal loading. The pelvis dimensions and soft tissue thickness of the anterior pelvis were carefully reviewed to represent the belt-pelvis interaction in the average body-size occupant. Three anthropometry models were generated: 5th-percentile adult female (AF05), 50th-percentile adult male (AM50), and 95th-percentile adult male (AM95). The geometry and material properties of the abdominal soft tissue, small intestine and mesentery were carefully defined to realistically reproduce the mechanical responses during the abdominal loading by referring to the loading test data on actual human tissues reported in the literature. The lumbar spine was also revised. Prior research has found that the lumbar spine receives a high load when the pelvis is firmly restrained to prevent disengagement of the lap belt in a reclined posture. The material properties of the intervertebral discs and spinal ligaments were carefully reviewed. The validity of the updated models was examined by comparing the mechanical responses with the test data from Post Mortem Human Subjects (PMHS). It was confirmed that the Version 7 responses generally matched the test data or fell within the test data variability. The validations were performed at both component and whole-body level by referring to the available test data.

## INTRODUCTION

In highly automated vehicles (autonomous driving level: four or higher), occupants are partially or fully freed from driving operations. It is expected that occupants may wish to ride in various seating arrangements and postures, and to spend their ride time in unconventional ways, such as relaxing, playing games, or working. Several studies have confirmed users' expectations for a more relaxing and comfortable ride by reclining their seats in future automated vehicles [1-2]. On the other hand, the vehicle crash tests conducted in the current regulatory compliance certification and the new car assessment programs basically assume the upright seat arrangement. In the reclining seat arrangement, there is a possibility that a vehicle collision occurs while the occupants are seated in a reclined posture. It is necessary to understand the effects on impact kinematics and possible injuries of such occupants during the collision. Various studies have been conducted for this purpose, such as collision tests using PMHS and vehicle collision simulations using HBMs. Discussions are underway to determine the effectiveness of the current restraint systems and future countermeasures to better protect the occupants.

The National Highway Traffic Safety Administration (NHTSA) has investigated occupant kinematics and injuries during frontal crashes in forward-facing and rear-facing reclined seat configurations [3-4]. Richardson et al. (2020) [5] conducted a 50 kph frontal sled test of a reclined PMHS to measure the occupant kinematics and injury responses. In the reclining posture, it was reported that the initial rearward pitch of the pelvis triggered disengagement of the lap belt from the anterior pelvis. As a result, the belt shifted up to the abdominal area

(called submarining). The lumbar spine was loaded by combined compression and bending as the upper body moved forward due to inertia. In recent years, many studies have been conducted using computer simulations with HBMs. The NHTSA has suggested that HBMs could be used in the future to confirm crash safety of automated vehicles in addition to physical testing [6]. It is expected to be used as a future evaluation tool taking advantage of the flexibility in posture change and higher biofidelity. Boyle et al. (2019) [7] investigated responses in frontal crashes for vehicle occupants in reclining posture through a simulation study using HBM. Their study results indicated that the submarining is more likely to occur as the reclining angle became larger. It was also indicated that the lumbar spine was subjected to higher load when the submarining was prevented by firmly restraining the pelvis. Similar results were reported in other studies on impact kinematics and injury outcomes of reclined occupants in vehicle frontal collisions [8-11].

HBMs are widely used for vehicle collision simulations in the field of occupant safety research. The HBMs are generally validated to PMHS test data to be used for prediction of impact kinematics and injury in vehicle collisions. In the previous research, the test conditions assumed an upright seating posture. Further validations are necessary to ensure the prediction accuracy of kinematics and injury in the reclining posture. As mentioned before, when the lap belt shifted up to the abdominal area (submarining) during a frontal collision, there is a possibility that the internal organs are loaded. There is another possibility that the lumbar spine is highly loaded if the submarining is prevented. Further validations are necessary for the prediction of abdominal organ damage and lumbar spine injury due to submarining, as suggested in previous studies. The current HBMs do not fully represent the complex geometry of the small intestine and mesentery but have a generic soft solid in the corresponding region. Such a simplified model does not accurately predict organ damage. Further validation is also necessary for the prediction of lumbar spine injury. This paper describes the development work of THUMS Version 7, which will be a major update of Version 6. The development targets are 1) to accurately predict the interaction between the pelvis and lap belt of a reclining occupant, and 2) to predict injuries to the internal organs and the lumbar spine in vehicle frontal collisions.

## MODEL DEVELOPMENT

### Overview of THUMS Version 7

THUMS is a series of virtual human body models that precisely represents the whole-body geometry and anatomical structures of the human body and reproduces the physical properties of the constituent tissues such as bones and internal organs. The development purpose was to simulate human body kinematics in vehicle collisions and to analyze crash-induced injuries. Figure 1 shows an overall view of the newly developed THUMS Version 7 occupant models. There are three body sizes equivalent to small female (AF05), midsize male (AM50), and large male (AM95). THUMS Version 4 [12], released in 2010, included detailed anatomic structures based on high-precision CT scan data to predict bone fractures, ligament tears, and brain and internal organ injuries. Version 5 [13], released in 2015, was a major update of Version 3 [14], released in 2008, with the addition of skeletal muscle models to simulate occupant postural changes prior to a collision. Version 6 [15], released in 2019, incorporated the muscle models into Version 4.

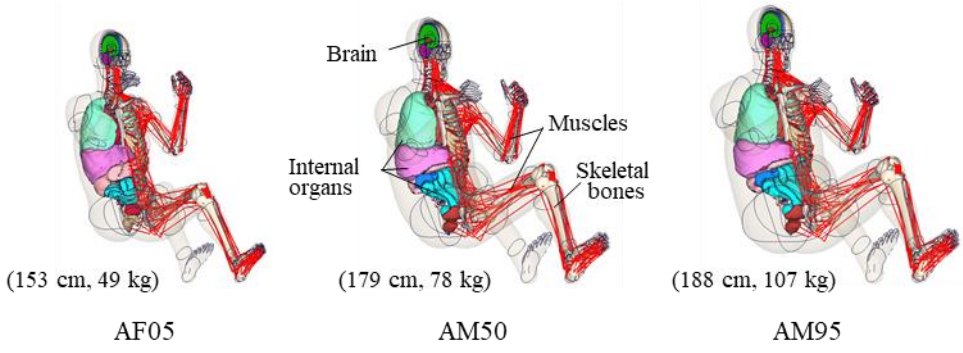


***Figure 1. Overall view of human body FE models (THUMS Version 7).***

Version 7 was developed based on Version 6 with significant improvements for injury simulation of occupants seated in a reclined position. One of the new features was the highly precise representation of the geometry and mechanical properties of the internal organs and lumbar spine. It was necessary to accurately reproduce the interaction between the pelvis and lap belt. Table 1 summarizes the modification items. The other features were the external geometry of the pelvis and abdomen, the physical properties of skin and adipose tissue, the structure of the small intestine and mesentery, and the characteristics of the intervertebral discs and ligaments of the spine. These new features contributed to accurate injury prediction. Modifications were also made to the regions other than the abdomen-pelvis. The detailed information is available in Appendix.
In the development work of Version 7, LS-DYNATM MPP971 R11.2.2 (Ansys, USA) was used to perform crash (dynamic loading) simulations. LS-DYNA is a general-purpose multi-physics simulation software package including a nonlinear explicit finite element solver.

**Pelvis Model**
The pelvis geometry was carefully reviewed to realistically reproduce submarining dependence on the seat reclining angle. Table 2 shows the measured mean ± standard deviation [16] and the pelvis dimensions for three body sizes (AF05, AM50, AM95). Version 6 AM50 was generated based on the CT scan data of an actual person whose body size was close to the midsize male. AF05 was generated using the same procedure. AM95 was scaled from AM50. The overall height ($h_{max}$), width ($w_{max}$), and depth ($d_{iliac}$) of the THUMS pelvises were at most 40 mm smaller than the mean size. The smaller size pelvis could underestimate the engagement of the lap belt and pelvis in vehicle frontal collision. To enhance prediction for the average result before considering individual differences, the Version 7 pelvis models were modified to match the average dimensions.

***Table 1.***
***Model generation and modification.***

| Body Region | Simulation target | Model generation and modification | Reference |
|---|---|---|---|
| Pelvis | Submarining | Pelvis geometry | [16] |
| Abdomen | | Abdominal skin geometry and property | [17-18] |
| | | Adipose tissue property | [19] |
| | Abdominal injury | Small intestine and mesentery models | [20-23] |
| Lumbar spine | Lumbar spine fracture | Intervertebral disc property | [23-24] |
| | | Ligament property | [25] |
| | | Cortical bone thickness of vertebrae | [26-28] |
| Others | Improvements for simulation accuracy (Refer to Appendix) | Head dimensions | [42] |
| | | Cortical bone thickness of ribs | [43] |
| | | Heart model | [45] |
| | | Long bone model | [23] |

***Table 2.***
***Pelvis geometry.***

| | AF05 | | | AM50 | | |
|---|---|---|---|---|---|---|
| | Measurement (Hwang, 2016) | THUMS V6 | THUMS V7 | Measurement (Hwang, 2016) | THUMS V6 | THUMS V7 |
| Wmax [mm] | 260 ±20 | 223 (-37) | 259 ( - 1) | 282 ±20 | 244 (-38) | 283 (+ 1) |
| Wisch [mm] | 119 ±13 | 115 ( - 4) | 117 ( - 2) | 98 ±10 | 96 ( - 2) | 96 ( - 2) |
| Hmax [mm] | 191 ±11 | 184 ( - 7) | 190 ( - 1) | 220 ±12 | 200 (-20) | 220 ( 0) |
| Hasis [mm] | 136 ±10 | 139 (+ 3) | 137 (+ 1) | 152 ±10 | 146 ( - 6) | 151 ( - 1) |
| Diliac [mm] | 135 ±8 | 131 ( - 4) | 136 (+ 1) | 148 ±11 | 133 (-15) | 148 ( 0) |
| Dasis [mm] | 11 ±4 | 11 ( 0) | 11 ( 0) | 10 ±5 | 4 ( - 6) | 10 ( 0) |

| | AM95 | | |
|---|---|---|---|
| | Measurement (Hwang, 2016) | THUMS V6 | THUMS V7 |
| Wmax [mm] | 286 ±20 | 261 (-25) | 285 ( - 1) |
| Wisch [mm] | 100 ±10 | 103 (+ 3) | 101 (+ 1) |
| Hmax [mm] | 226 ±12 | 214 (-12) | 225 ( - 1) |
| Hasis [mm] | 155 ±10 | 156 (+ 1) | 155 ( 0) |
| Diliac [mm] | 151 ±11 | 142 ( - 9) | 151 ( 0) |
| Dasis [mm] | 11 ±5 | 4 ( - 7) | 11 ( 0) |

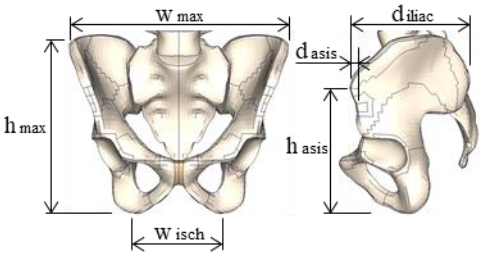


**Abdominal Model**

The geometry and mechanical properties of the soft tissues (skin, adipose) of the anterior abdomen were revised. The soft tissue on the anterior aspect of the Anterior Superior Iliac Spine (ASIS) of the pelvis greatly influences the interaction with the lap belt. Table 3 summarizes the mean numbers of soft tissue thickness for each body sizes [17] with a comparison of THUMS dimensions. The soft tissue thickness values of Version 6 AM50 and AM95 were larger than the mean numbers. In Version 7, these thickness values were modified to approach the mean numbers. During the mesh modification work, the quality of the solid elements was monitored so as not to be degraded (aspect ratio < 5). The modification reduced the discrepancy between the thickness values and the mean numbers to about ±10 mm.

Figure 2 shows the tensile properties of the skin. The material model of the Version 6 skin assumed a linear elastic material. Compared to human skin data [18], the modulus was higher up to a strain of 0.5 and lower after that region. In Version 7, nonlinear characteristics were defined for the skin material in order to better represent the human skin tissue. Annaidi et al. (2013) [18] found that the mean modulus of elasticity of the skin depends on the orientation of the Langer line. The modulus in the vertical direction is lower than that in the parallel direction. When the lap belt loads the abdomen, the skin tissue is pulled in the direction perpendicular to the Langer line. The modulus of the skin properties in Version 7 was adjusted to the lower limit of the test data.

When the lap belt disengages from the pelvis, the adipose tissue in front of the iliac crest exhibits compressive and shear deformation modes simultaneously. Sun et al. (2021) [19] experimentally determined the compression and shear properties of the adipose tissue at three levels of strain rate (3, 13, and 50 $s^{-1}$). Figure 3 superimposes the average properties and corridors obtained from the tests and the compression and shear properties of the THUMS adipose tissue model. The Stress-Strain properties of the Version 7 material model (hyper-elastic) were set so that the properties in compression and shear at each strain rate were close to the average properties from the tests.

***Table 3.***
***Abdominal skin geometry.***

| | Soft tissue thickness in front of ASIS [mm] | | |
|---|---|---|---|
| | UMTRI | THUMS V6 | THUMS V7 |
| AF05 | 29 | 16 (-13) | 16 ( -13) |
| AM50 | 20 | 60 ( +40) | 19 ( - 1) |
| AM95 | 35 | 90 ( +55) | 45 ( +10) |

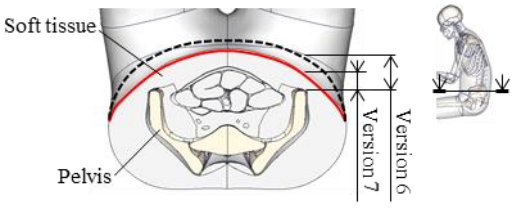

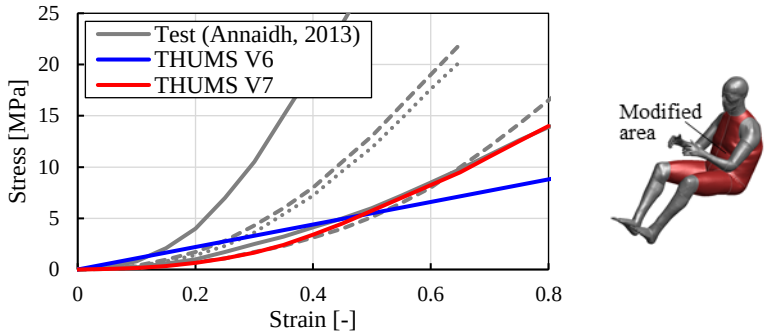


***Figure 2. Abdominal skin property.***

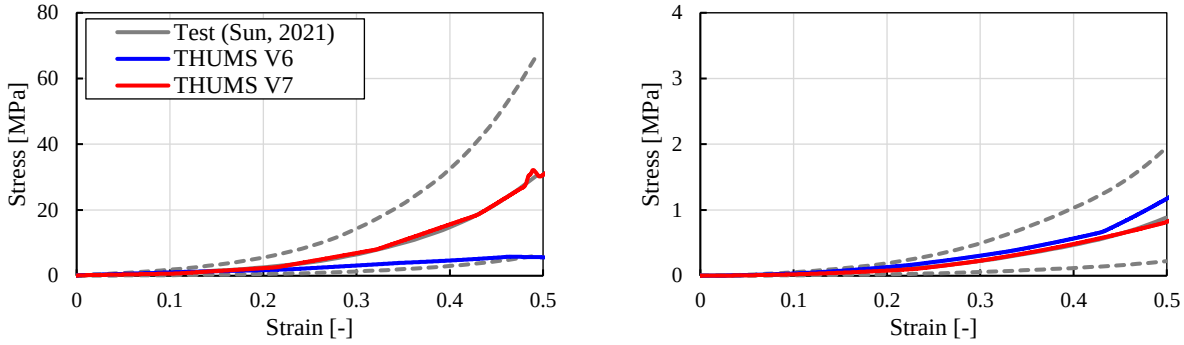


(a) Compression (strain rate: $3s^{-1}$)




(d) Shear (strain rate: 3 $s^{-1}$)

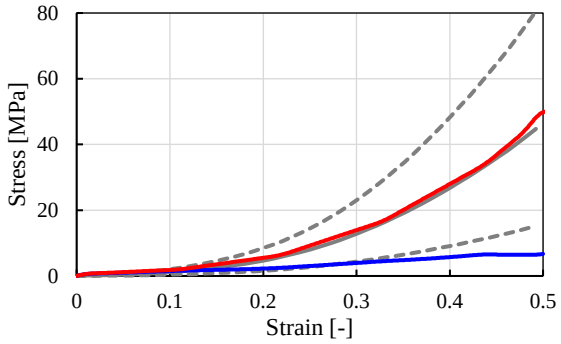


(b) Compression (strain rate: 13 $s^{-1}$)

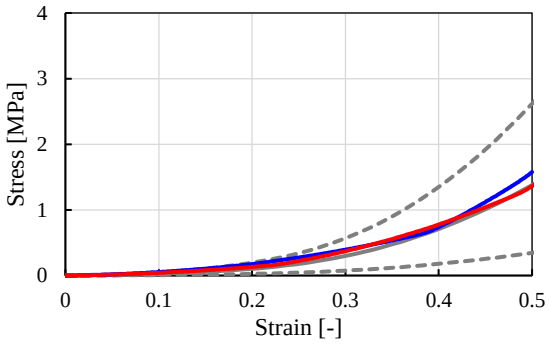


(e) Shear (strain rate: 13 $s^{-1}$)

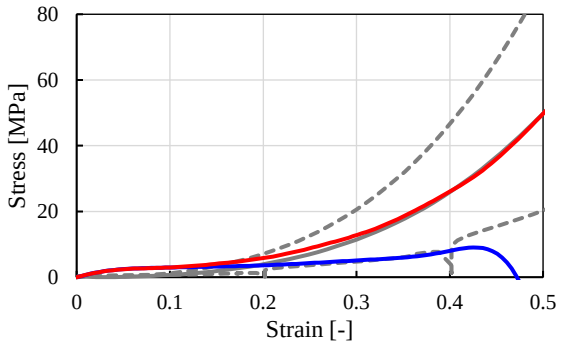


(c) Compression (strain rate: 50 $s^{-1}$)

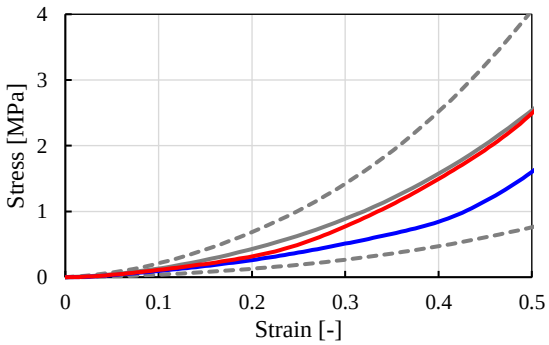


(f) Shear (strain rate: 50 $s^{-1}$)

***Figure 3. Adipose tissue property.***

**Small Intestine and Mesentery Model**

In order to analyze injuries of the small intestine and mesentery, the anatomical structures and characteristics of the small intestine and mesentery were more accurately reproduced in Version 7. Figure 4 shows the small intestine models of Version 6 and Version 7. In Version 6 (as well as Version 4), the small intestine was represented as a simplified homogeneous structure which was different from the anatomic structure of the small intestine and mesentery. In Version 7, the long and folded intestinal geometry, mesentery, and intramesenteric vessels were precisely represented in the abdominal region [20]. In finite element modeling, shell elements were used to replicate the intestinal tract as a tubular part with a diameter of approximately 20 mm. The inside of the tube was filled with solid elements to mimic the contents. Based on tensile measurement data of the actual human tissue [21], a transverse anisotropic nonlinear elastic material with different properties in the axial and circumferential directions was defined for the intestinal part (Figure 5). For the solid part, the same material properties as the Version 4 small intestine model were used, assuming a foam material with nonlinear compressive properties. The mesenteric model was generated as a lattice mesh structure with contractible beam elements. Shell elements were added to fill the interstices of the mesh for contact calculations. The mesenteric vascular was also replicated by connecting beam elements using the nodes of the mesh forming the mesenteric model. Nonlinear elastic materials were defined for the mesenteric beam elements based on the tensile test data of the human gastric serosa [22]. Null material with no deformation resistance was applied to the shell elements in the mesenteric part for contact calculations. For the beam elements of the intramesenteric vessels, nonlinear elastic materials were defined based on the tensile test data of the human abdominal aorta [23].

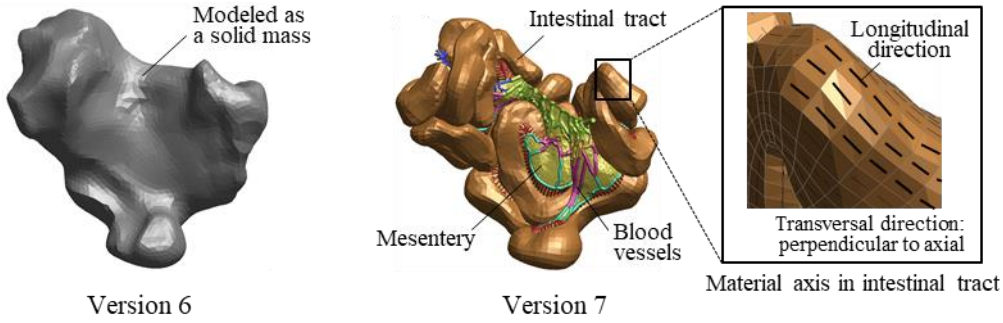


***Figure 4. Small intestine model.***

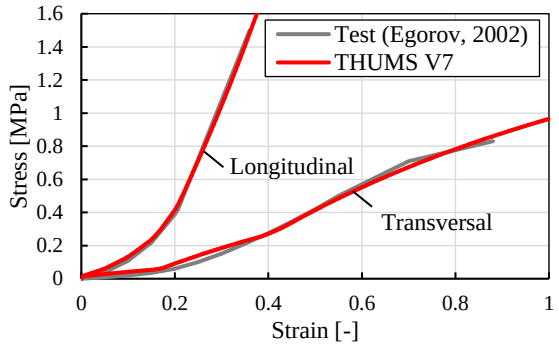


***Figure 5. Tensile properties of intestinal tract.***

**Lumbar Spine Model**

The lumbar spine part was also updated in Version 7. The mechanical properties of the intervertebral disc and the ligaments around the spine were carefully reviewed. A nonlinear foam material was defined for the intervertebral discs based on the quasi-static (strain rate: $0.01s^{-1}$) compression test data [23] of the actual human tissue. Kemper et al. (2013) [24] identified the relationship between strain rate and disc stiffness (Equation (1)). Based on the relationship, the rate of increase in stiffness at strain rates of 5.3, 12.1, and 73.7 $s^{-1}$ were calculated. The intervertebral disc properties in Version 7 were determined by scaling the stress-strain characteristics of the quasi-static compression (Figure 6).

$$k = 57.328\,\dot{\varepsilon} + 2019.1 \qquad \textit{Equation (1)}$$

$$k: Stiffness\ (N/mm),\ \ \dot{\varepsilon}: Strain\ rate\ (s^{-1})$$

There are multiple ligaments attached around the spine. Those ligaments contribute to the mechanical properties of the spine. In Version 6, linear elastic properties were assumed for the ligaments. In Version 7, nonlinear elastic properties were adopted in order to more accurately simulate the tensile properties of actual ligaments [25]. The nonlinear properties were approximated by three straight lines (Figure 7). For the Intertransverse ligament (ITL) and Facet capsular ligament (CL), for which no reference data are available, the average numbers of Anterior longitudinal ligament (ALL), Interspinous ligament (ISL), Supraspinous ligament (SSL), Posterior longitudinal ligament (PLL) and Ligamentum flavum (LF) were defined for the property.

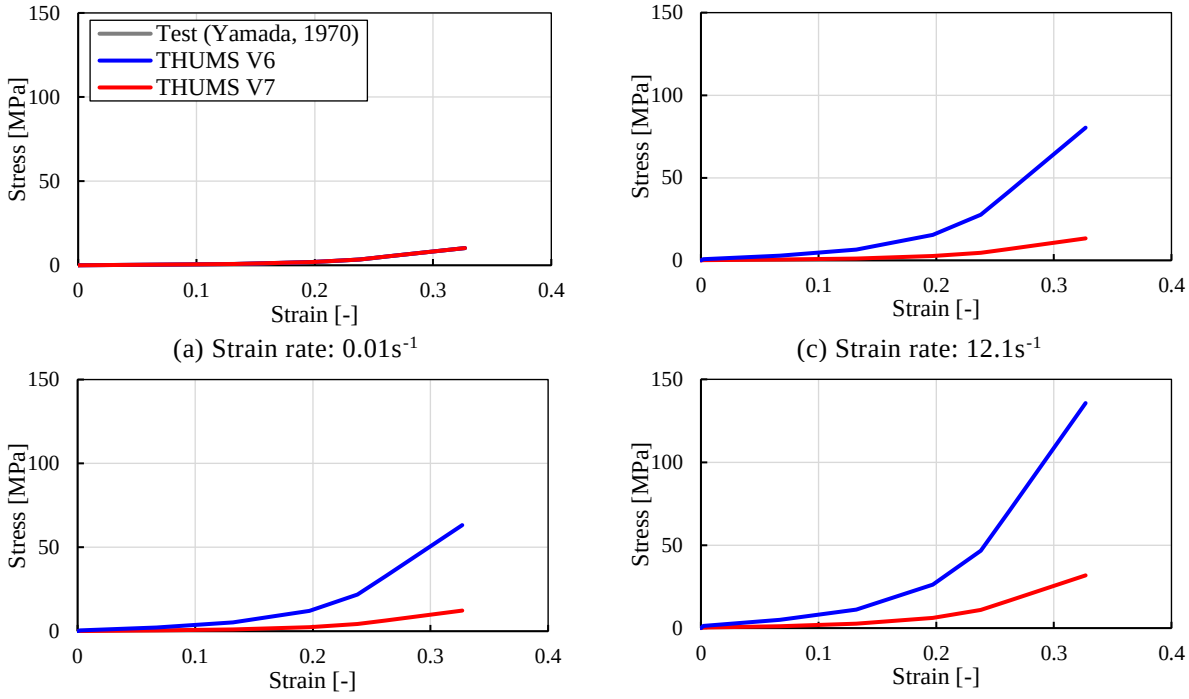


(a) Strain rate: $0.01s^{-1}$ (c) Strain rate: $12.1s^{-1}$

(b) Strain rate: $5.3s^{-1}$ (d) Strain rate: $73.7s^{-1}$

***Figure 6. Intervertebral disc property.***

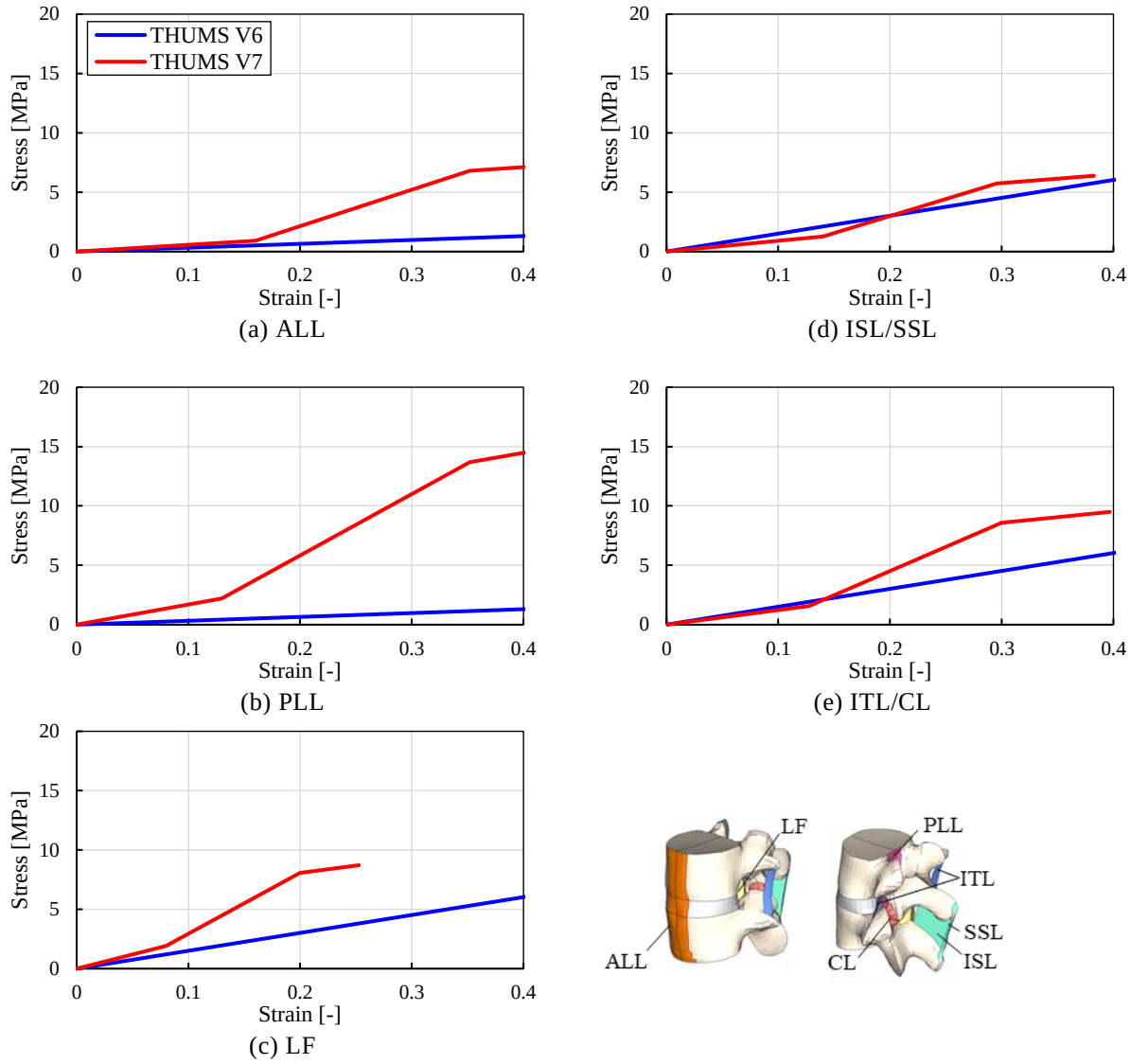


***Figure 7. Ligament property***

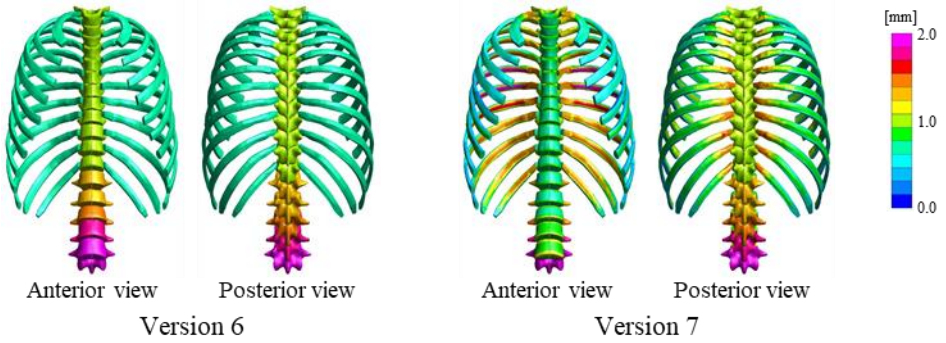


***Figure 8. Cortical bone thickness distribution of vertebrae.***

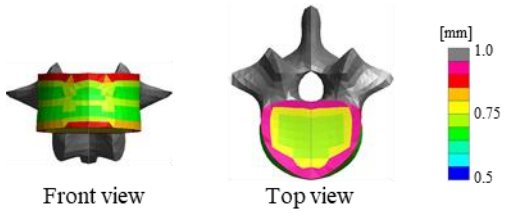


***Figure 9. Cortical bone thickness distribution of L1 vertebra.***

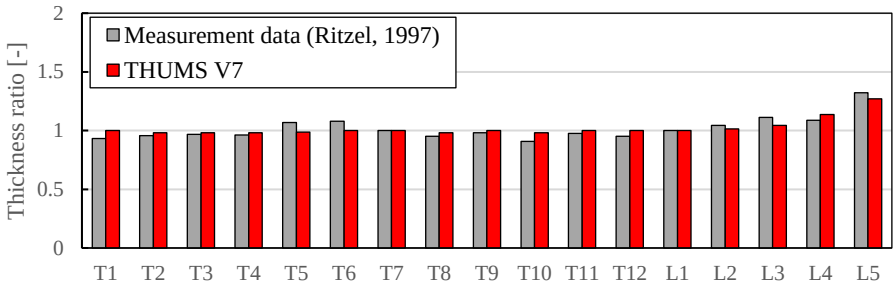


***Figure 10. Ratio of cortical bone thickness to L1 vertebra.***

In Version 6, a uniform thickness was assumed for the cortical bone of all vertebrae. In Version 7, uneven distribution of thickness was incorporated into the cortical bone of each vertebra (Figure 8). The realistic thickness distribution contributes to accurate prediction of vertebral fractures. First, the thickness distributions of the lateral and vertical walls of the vertebral bodies were determined based on the measurement data of the actual human L1 [26-27]. For the areas other than the vertebral body, such as the vertebral arch and spinous process, the cortical bone thickness was assumed to be uniform. The same thickness values as Version 6 were used for Version 7 (Figure 9). For the other vertebrae in the lumbar spine and thoracic spine, the cortical bone thickness of each vertebra was determined by calculating the thickness ratio of each vertebra to that of L1, based on the measured data of the cortical bone thickness of the front surface of the vertebra [28] (Figure 10). The thickness distribution of the cortical bone from T1 to L1 was assumed to be the same. The thickness of the cortical bone of L5 was assumed to be 1.27 times greater than that of L1. It was assumed that the thickness gradually increased from L1 to L5. The thickness of the cervical spine was not changed from Version 6.

## MODEL VALIDATION

The validity of the mechanical responses of THUMS Version 7 were examined by comparing with PMHS tests described in the literature. The results were also compared with Version 6 results to confirm the effects of the model modifications. First, the model was validated for each component unit of the abdomen and lumbar region, and then the whole-body kinematics were verified under vehicle frontal impact conditions. In the component validation for the pelvis and abdomen, both ends of the lap belt were towed backward to replicate a sliding motion on a reclined occupant in a vehicle frontal collision. The load response characteristics were also examined under other conditions. The mechanical properties of the Functional Spine Unit (FSU) and the entire lumbar spine from L1 to L5, were validated in the combined loading of bending and shear. Finally, using a whole-body model seated in a reclining posture, the impact kinematics was examined by monitoring the displacement and trajectory of target points on the body. The impact condition assumed a vehicle frontal collision. The THUMS results were compared with the PMHS test data reported in the literature. Table 4 summarizes the validation cases.

***Table 4.***
***Model validation cases.***

| Body Region | | Model validation | Reference |
|---|---|---|---|
| Component | Pelvis | Interaction between pelvis and lap belt | [29] |
| | Abdomen | Load response of abdomen | [30-34] |
| | | Abdominal organ injuries | [30-34] |
| | Lumbar spine | Characteristics of lumbar spine [FSU] | [35-36] |
| | | Characteristics of lumbar spine [L1-L5] | [37] |
| | | Lumbar spine fractures | [38] |
| | Others (Refer to Appendix) | Rib fractures | [44] |
| | | Load response of heart | - |
| | | Bending stiffness of long bone | [23] |
| Whole-body | | Kinematics during frontal collision in forward-facing reclined seating | [3,39] |

**Component Validation**

**Interaction between pelvis and lap belt** Richardson et al. (2021) [29] conducted PMHS tests to monitor the lap belt motion and load response when the engagement with the pelvis was lost and the lap belt slid up causing the submarining. Figure 11 shows a schematic view of the simulation model. The subject was an adult male with a height of 183 cm and a weight of 104 kg. The THUMS AM95 model (188 cm, 107 kg) was selected for comparison. The thoracic, lumbar, and sacral vertebrae were rigidly connected to the support column, which was reclined 45 degrees from the vertical as support conditions equivalent to those in the test. Both legs were supported to make the femur angle inclined by approximately 15 degrees from the horizontal line. The lap belt was draped over ASIS and Anterior Inferior Iliac Spine (AIIS) and was adjusted so that the angle between the ASIS-AIIS line and the lap belt became 74 degrees which was the average in the tests. Both ends of the lap belt were connected to steel cables and pulled rearward with a prescribed displacement of approximately 140 mm (Figure 12).
Figure 13 shows the trajectory of the center of the lap belt calculated from the simulation using Version 7. It was close to the trajectory measured in the test. Figure 14 shows the lap belt tension vs. X displacement diagram of the center of the belt. Version 6 generated a higher load by 2 kN compared to the test data. The calculated load in Version 7 was closer to the test data. In addition, the load-displacement characteristics after the disengagement of the lap belt in Version 7 were closer to those of the tests compared to Version 6.

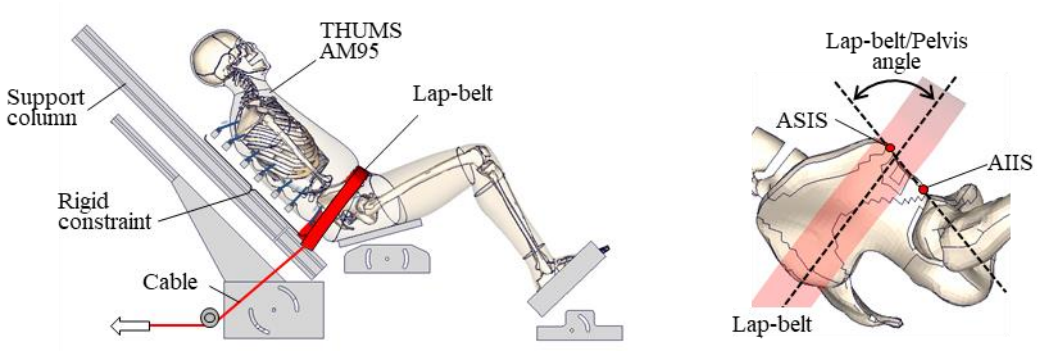


***Figure 11. Simulation model of lap belt loading to pelvis.***

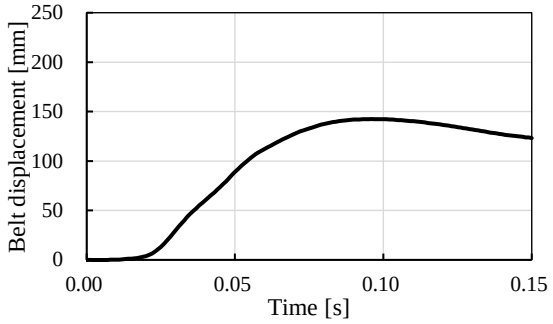


***Figure 12. Lap belt displacement pulse.***

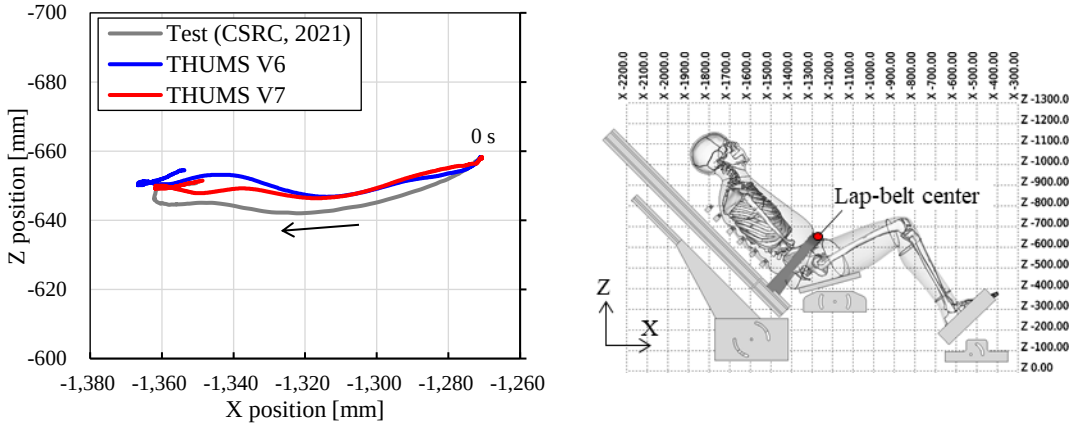


***Figure 13. Trajectories of center point of lap belt.***

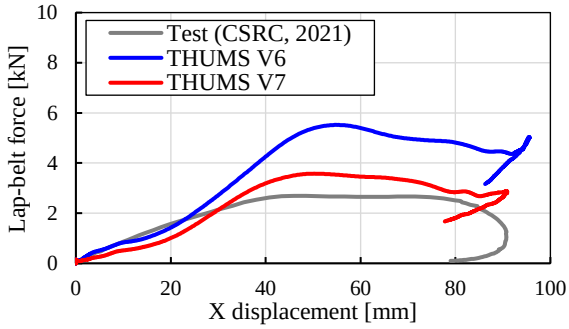


***Figure 14. Lap belt force vs. X displacement curves.***

**Load response of abdomen** The validation for the abdominal model was conducted by applying compressive load under various conditions. Table 5 summarizes the loading conditions. Figure 15 shows a schematic view of the simulation models. A total of six cases were simulated: three cases with rigid impactors (Cases-i1, i2, i3) [30-32] and another three cases with seat belts (Cases-b1, b2, b3) [32-34]. The loading conditions in the simulation models, such as impactor geometry, mass, initial velocity and belt position, and velocity history were set to be equivalent to those in the tests. In each case, the THUMS model was selected whose body size was close to the average of the test subjects. The AF05 model was used in Case-b1, while the AM50 model was used in the other cases.
Figures 16 (a)-(c) show the results of the load-deflection diagrams under the impactor loading conditions. In Case-i1, the load output from Version 7 was within the test corridor from the start of loading up to a deflection of 100 mm.

After that, the Version 7 load slightly exceeded the upper boundary of the corridor. In Case-i2 and Case-i3, the loads output from Version 7 were within the variability of the test results over almost the entire range of loads applied. Figures 16 (d)-(f) show the results of the load-deflection (Case-b2: lap belt displacement) diagram under the belt loading conditions. In Case-b1, the maximum load value and the deflection at that time output from Version 7 were within the test corridor. The Version 7 load was partially below the lower boundary of the test corridor in the deflection range below 50 mm. In Case-b2, the maximum load value output from Version 7 was close to the test results. The calculated load-deflection diagram up to the maximum peak was lower than the test results. In Case-b3, the maximum load value, the deflection at that time and the curve after turning to unloading output from Version 7 were within the test corridor. The initial load rise at the deflection range below 10 mm was higher than the upper boundary of the test corridor.

***Table 5.***
***Validation cases of abdominal loading.***

| Case No. | Load type | Load conditions (speed, mass) | THUMS physique | Reference |
|---|---|---|---|---|
| Case-i1 | Rigid-bar impact | 6.1m/s, 32kg | AM50 | [30] |
| Case-i2 | Rigid-steering impact | 10m/s, 18kg | AM50 | [31] |
| Case-i3 | Rigid-bar impact | 9.0m/s, 48kg | AM50 | [32] |
| Case-b1 | Seatbelt loading | 3.0m/s, - | AF05 | [32] |
| Case-b2 | Seatbelt loading (lap & shoulder) | 3.0m/s, - | AM50 | [33] |
| Case-b3 | Seatbelt loading | 6.9m/s, - | AM50 | [34] |

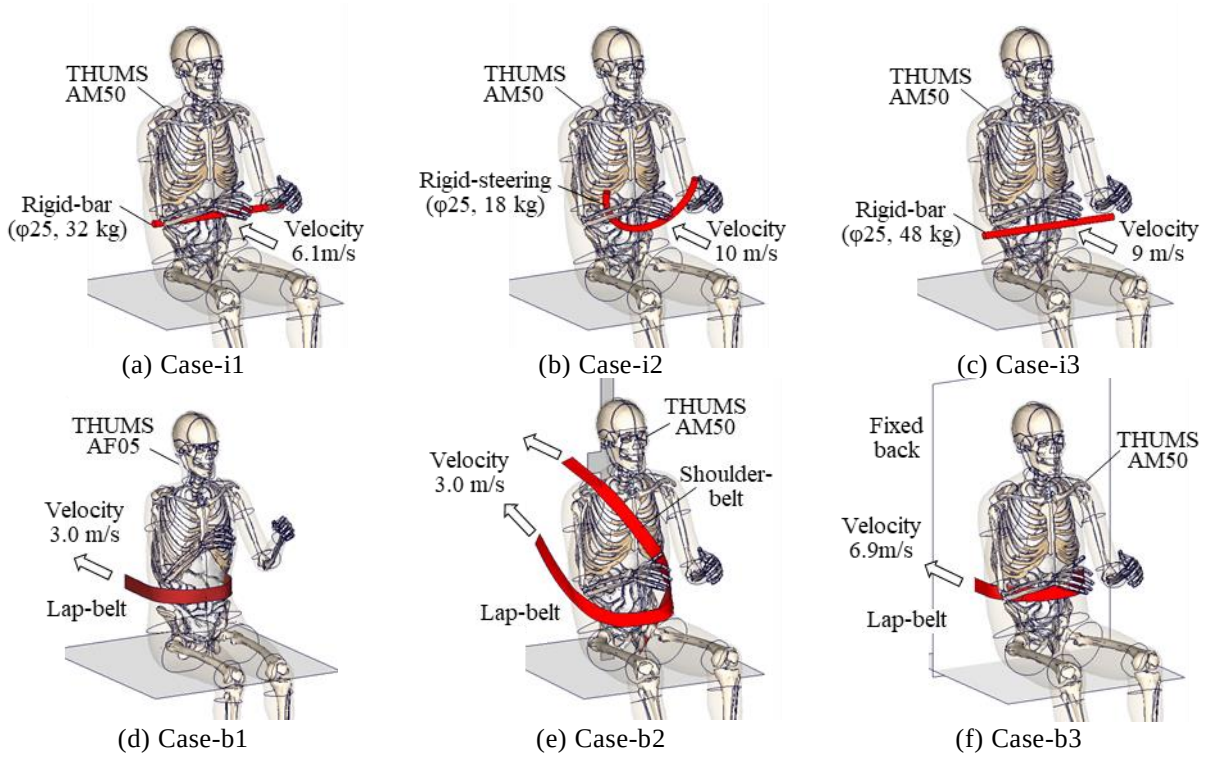


***Figure 15. Simulation models of abdominal loading.***

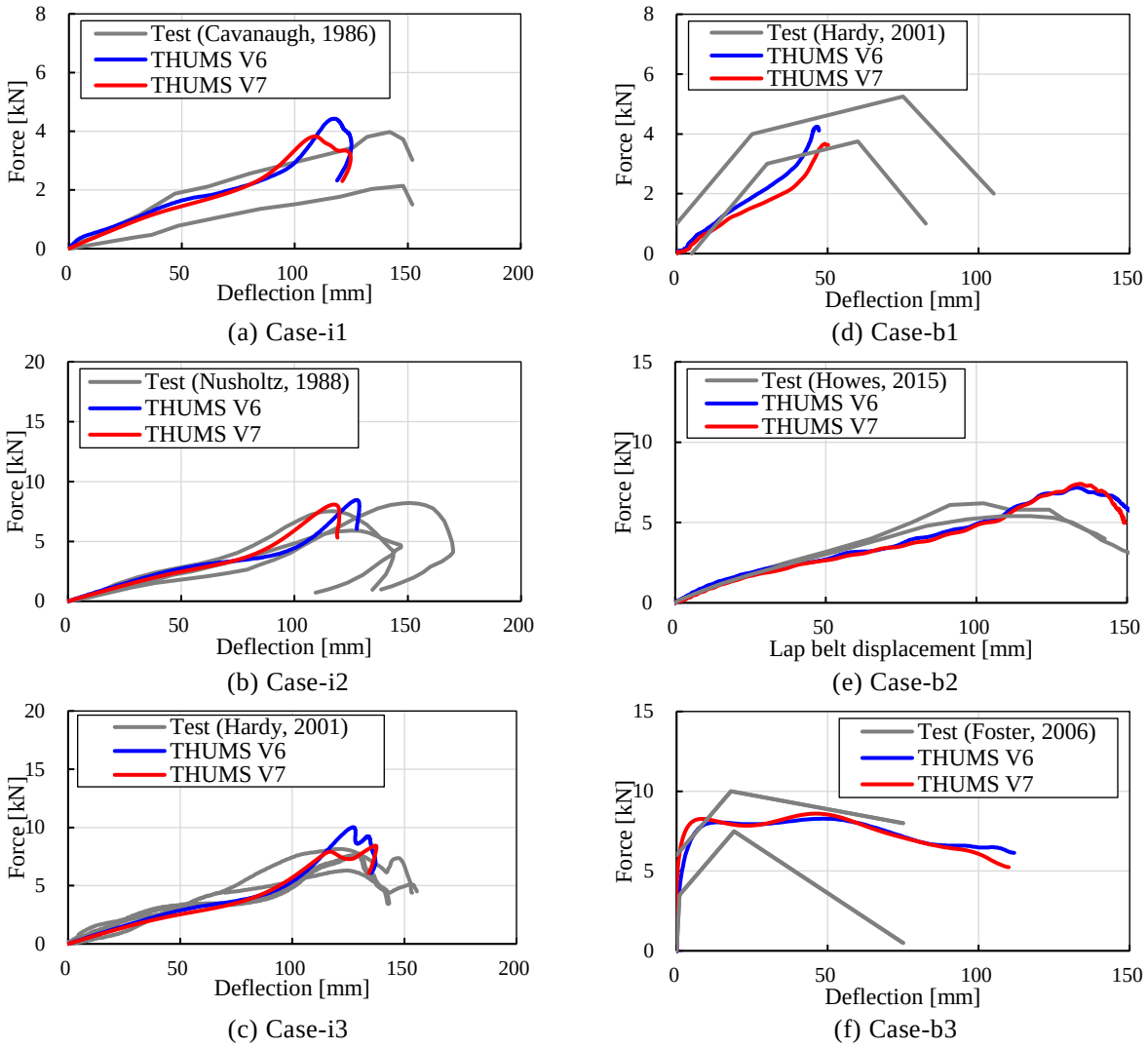


***Figure 16. Impactor and belt force vs. abdominal deflection curves.***

**Abdominal organ injuries** The mechanical properties of the abdominal part were validated in six loading cases. Table 6 summarizes the maximum strain values calculated in the shell and beam elements of the intestinal tract, mesentery, and mesenteric vessels. Table 6 also shows the measured values of the rupture strain obtained from tensile tests of the intestinal tract [21], mesentery [22], and vessels [23]. The amounts of energy applied to the abdomen are also shown in the same table. In this validation, the rupture strain values of the intestine in the axial and circumferential directions were tentatively assumed to be 0.37 and 0.88, respectively. The maximum strain values calculated from the intestine model were lower than the thresholds in all cases. In the simulations, the calculated strain value was lowest in Case-b2, while intestinal rupture occurred in both axial and circumferential directions in the test corresponding to Case-b2. The calculated strain values of the mesenteric exceeded the threshold in all cases. On the other hand, the mesentery was not damaged in all test cases. The calculated strain value of the vascular was highest in Case-i2. There was no description of vascular injury in the literature.

***Table 6.***
***Maximum strain of intestinal tract, mesentery and blood vessel.***

| Case No. | Maximum strain [-] | | | | Loaded energy [J] |
|---|---|---|---|---|---|
| | Intestinal tract | | Mesentery | Blood vessel | |
| | Longitudinal | Transversal | | | |
| Threshold (Rupture strain) | 0.37 | 0.88 | 0.44 | 0.94 | - |
| Case-i1 | 0.36 | 0.56 | 1.00 | 0.72 | 234 |
| Case-i2 | 0.35 | 0.73 | 1.10 | 0.98 | 395 |
| Case-i3 | 0.36 | 0.64 | 1.37 | 0.96 | 530 |
| Case-b1 | 0.33 | 0.73 | 0.70 | 0.64 | 80 |
| Case-b2 | 0.32 | 0.73 | 0.91 | 0.70 | 567 |
| Case-b3 | 0.36 | 0.56 | 1.09 | 0.85 | 846 |

**Characteristics of lumbar spine [FSU]** The mechanical properties of the lumbar spine model were examined. First, the compressive and shear/bending properties of the FSU were checked, then the shear and bending properties of the entire lumbar spine were verified.

Arun et al. (2017) [35] performed a compression test to the FSU of L1-L2. A simulation model was generated to reproduce the test. The upper and lower vertebrae were potted to the cups so that the neutral plane of the disc was perpendicular to the direction of compression. The lower potting cup was restrained and the upper one was compressed with a downward velocity of 1.0 m/s. The load-displacement characteristics were compared between the test and simulation (Figure 17(a)). Belwadi et al. (2008) [36] performed a test on T12-L2 applying a combined load of shear and bending. The upper vertebrae were potted and restrained at a position where the center of gravity of the lower vertebrae coincided with the center of the lower potting cup and the top of the upper vertebral end plate was parallel to the top of the lower potting cup. The lower potting cup was restrained and the upper one was loaded with a displacement of 4 mm/s in the horizontal forward direction and a rotation of 0.061 rad/s in the forward flexion direction simultaneously. Another simulation model was generated to reproduce the test (Figure 17(b)). The calculated load-displacement and moment-angle characteristics were compared to those measured in the test. Figure 18(a) shows the load-displacement diagram in compression. Figures 18(b-1) and (b-2) show the shear load-shear displacement and forward bending moment-deformation angle diagrams in flexural shear. The load-displacement curve calculated by Version 7 was within the test corridor while that by Version 6 was higher than the upper boundary. The stiffness in shear and flexion output from Version 7 was also lower than in that from Version 6. The shear load, displacement, moment and angle, calculated by Version 7, at the timing of fracture prediction (cortical bone plastic strain ≥2%) were within the variation of the test data.

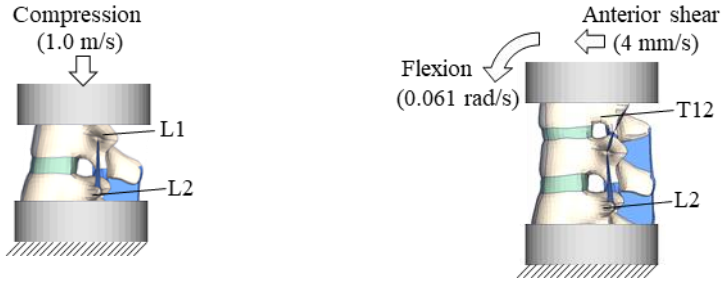


(a) Compression (b) Flexion/shear

***Figure 17. Simulation models of FSU loading.***

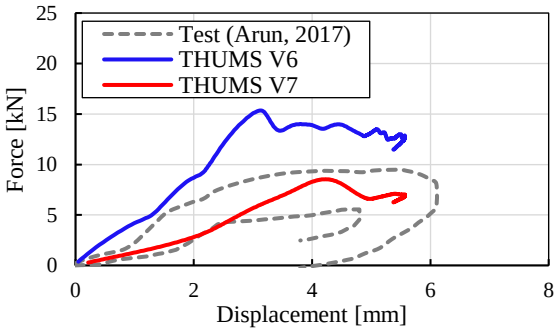


(a) Compression force - displacement

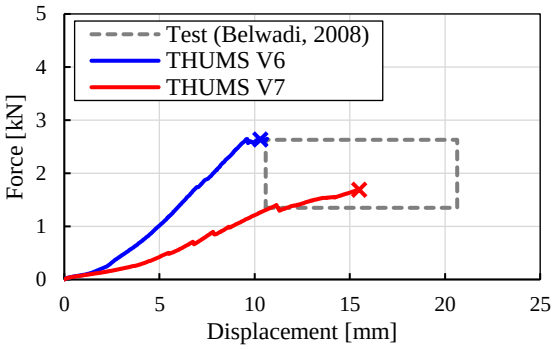


(b-1) Anterior shear force – displacement

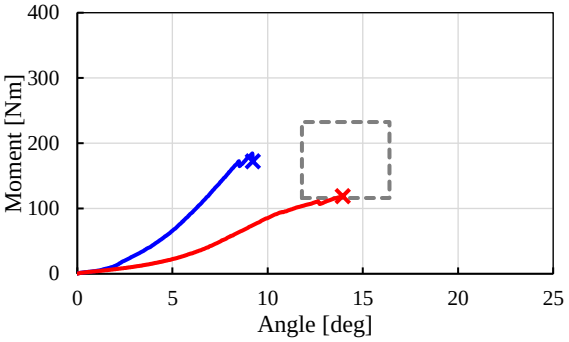


(b-2) Flexion moment - angle

***Figure 18. Compressive force vs. displacement (a) and anterior shear force vs. displacement, flexion moment vs. angle curves (b-1, b-2).***

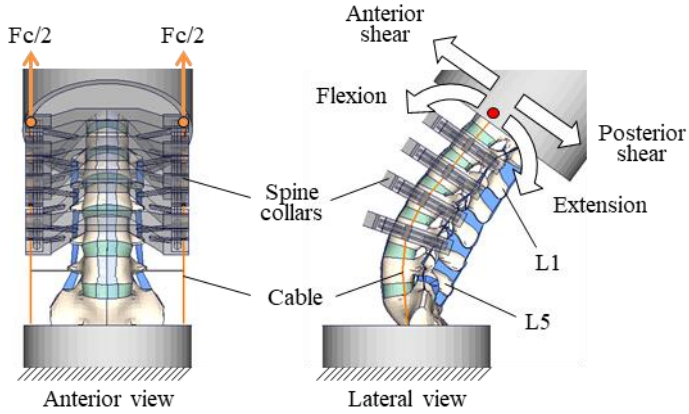


***Figure 19. Simulation model of lumbar spine loading.***

***Table 7.***
***Validation cases of lumbar spine loading.***

| Direction | Compression load | | |
|---|---|---|---|
| | 0 N | 900 N | 1800 N |
| Flexion | Case-fl0 | Case-fl9 | Case-fl18 |
| Extension | Case-ex0 | Case-ex9 | Case-ex18 |
| Anterior shear | Case-as0 | Case-as9 | Case-as18 |
| Posterior shear | Case-ps0 | Case-ps9 | Case-ps18 |

**Characteristics of lumbar spine [L1-L5]** The mechanical properties of the entire lumbar spine model were verified. Chastain et al. (2021) [37] conducted a bending and shear test to the lumbar spine from T12 to S1. The section was cut from T12 to S1, and soft tissues other than the posterior ligament tissue were excluded. T12 and S1 were potted in a cup and the potting cup on the S1 side was completely restrained. Collars (with a beacon marker for kinematics measurement and a mechanism for adjusting the anterior-posterior position of the cable) were attached to L1 to L4 as in the test. The cables were pulled through both sides of the collars, and a compressive load was applied in the axial direction of the lumbar spine. Bending (flexion/extension) and shear (anterior/posterior) characteristics were investigated at compressive loads of 0, 900, and 1800 N, respectively. The loading rates in bending and shear were 3 deg/s and 50 N/s. The upper potting cup was operated in such a way that the change in compression load and shear load was zero in the bending test and zero in the shear test. Displacements and angles were measured in the upper potting cup, and loads and moments were measured in a section set horizontally in the lower potting cup. A simulation model was generated to reproduce the test. Figure 19 shows a schematic view of the simulation model. Table 7 summarizes the simulation cases. Figure 20 shows the calculated the moment-angle curves in flexion and extension. The simulation results in the flexion cases (Case-fl series) slightly exceeded the upper limit of the test corridors in the region above about 20 degrees. The calculated flexion properties and moment-angle characteristics in the extension cases (Case-ex series) were generally within the test corridors.

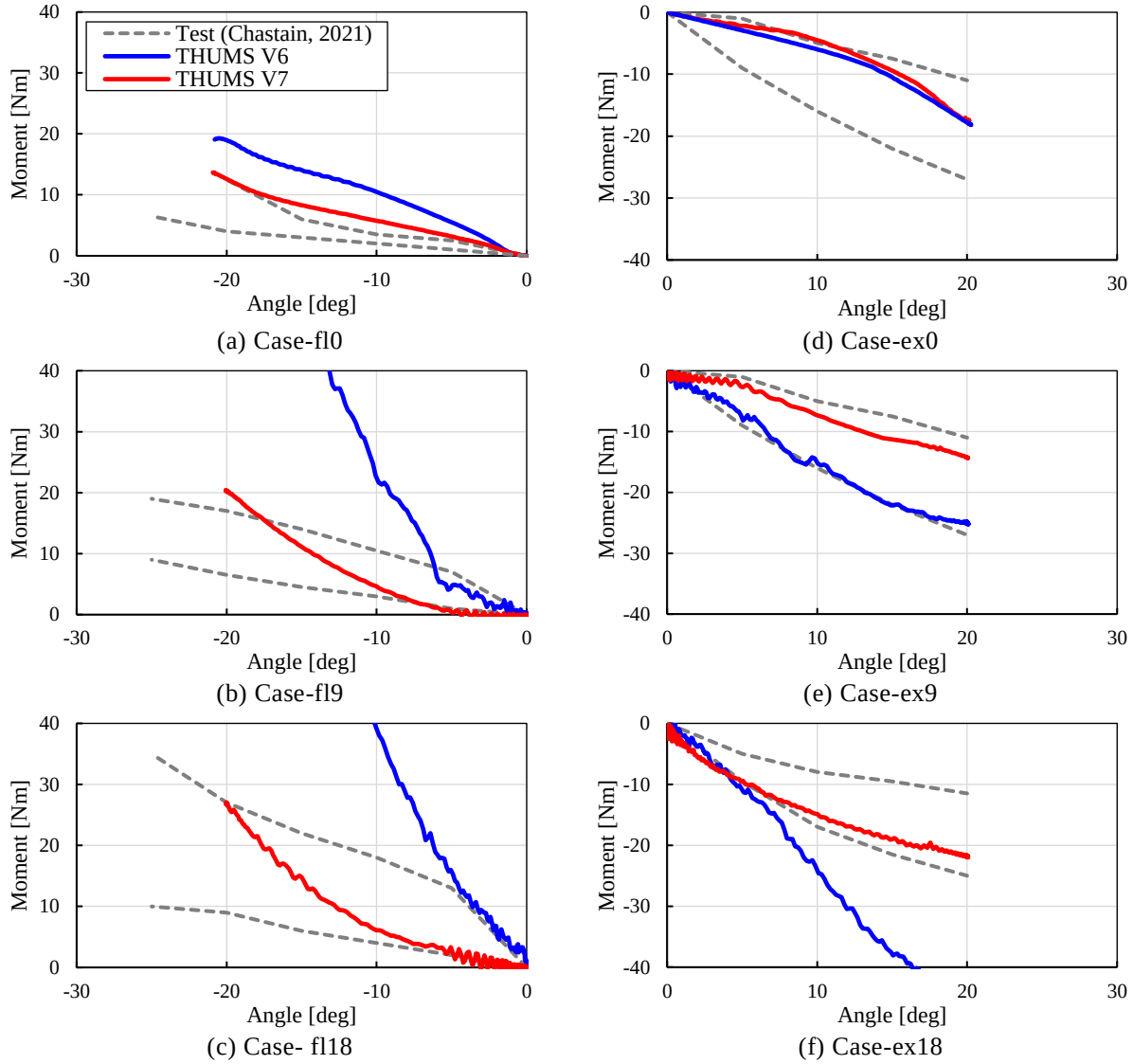


***Figure 20. Flexion and extension moment vs. angle curves.***

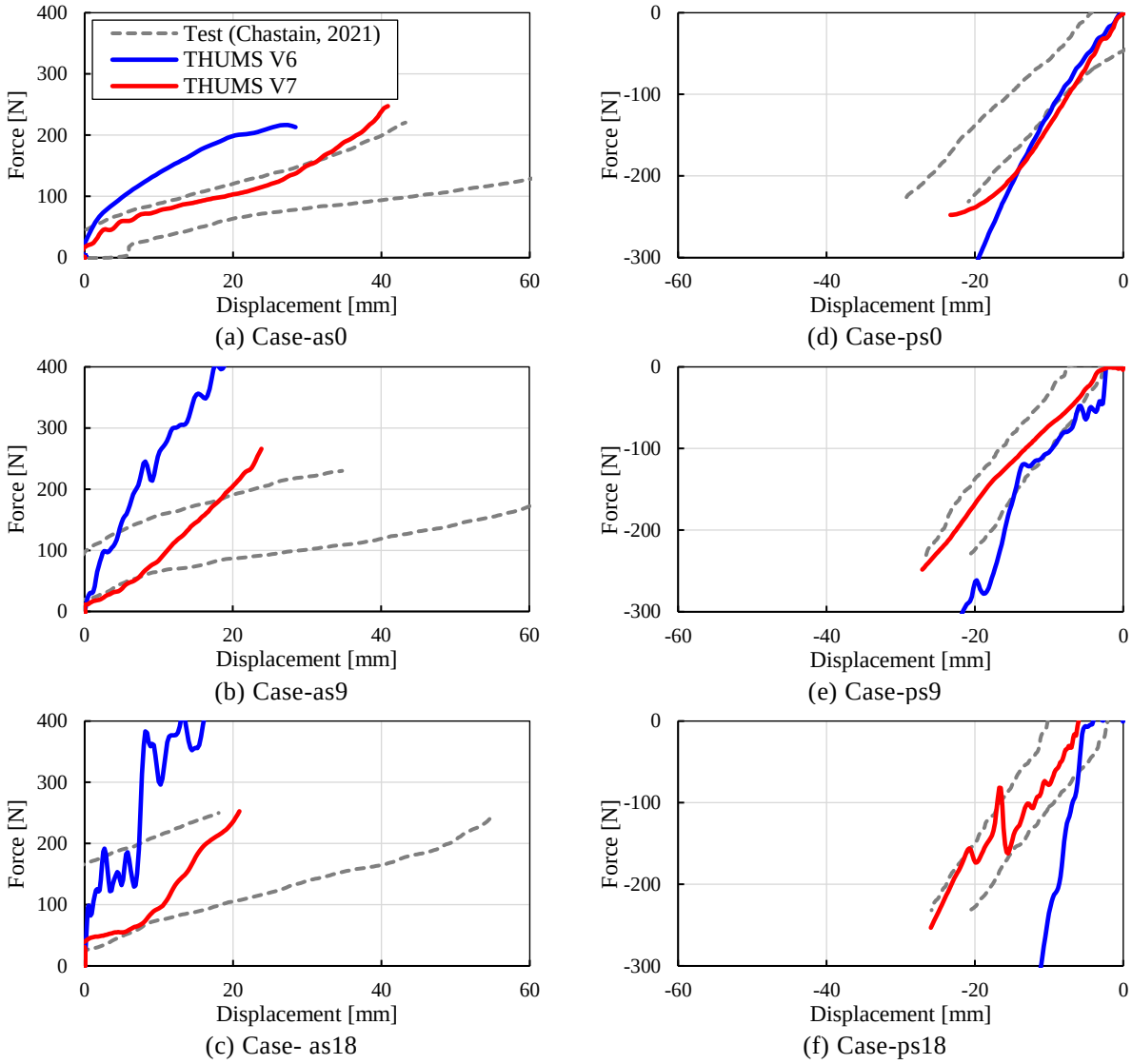


***Figure 21. Anterior and Posterior shear force vs. shear displacement curves.***

Figure 21 shows the shear load-displacement characteristics in anterior and posterior shear. The simulation results in the anterior shear cases (Case-as series) were higher than the upper boundary of test corridors for the displacement range of 20~30 mm. The calculated curves for the other range remained within the test corridors. The calculated shear load-displacement characteristics in the posterior shear cases (Case-ps series) were almost fully within the test corridors.

**Lumbar spine fractures** The prediction accuracy of vertebral fracture under combined compression and bending loading conditions was examined. Tushak et al. (2022) [38] conducted a test applying compression and flexion to FSU. Two FSU segments, upper (T12-L2) and lower (L3-L5), were extracted and the upper and lower vertebrae were fixed with potting cups. Compressive loads (three cases: 2200, 3300, and 4500 N) were applied quasi-statically to the lower potting cup, and then the upper potting cup was flexed forward at an angular velocity of 10.47 rad/s to apply bending loads. Simulation models were generated to reproduce the tests (Figure 22). Table 8 summarizes the calculation cases. The calculated loads and moments at which vertebral fractures were predicted by the simulation model were compared with the test results. It was assumed that fracture occurred when the plastic strain of the cortical bone exceeded 2%. Figures 23 (a) and (b) compare the load and moment at fracture in the upper and lower segments

of lumbar spine between the simulation and the test. In Version 6, the calculated moment in the lower segment was higher than the test variation range. In Version 7, the calculated moment was close to the upper boundary of the test variation. The magnitude of load and moment at fracture prediction was within the test variation for both the upper and lower segments.

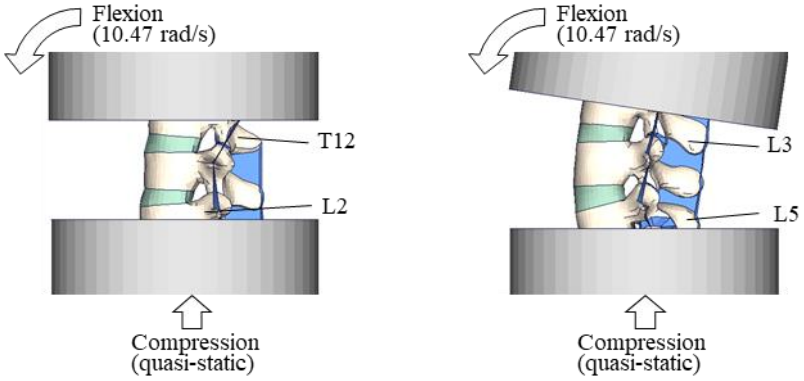


(a) Upper segment (b) Lower segment

***Figure 22. Simulation models of FSU loading to validate* vertebral *fracture.***

***Table 8.***
***Validation cases of FSU loading to validate vertebral fracture.***

| Segment | Compression load | | |
|---|---|---|---|
| | 2200 N | 3300 N | 4500 N |
| Upper | Case-u22 | Case-u33 | Case-u45 |
| Lower | Case-l22 | Case-l33 | Case-l45 |

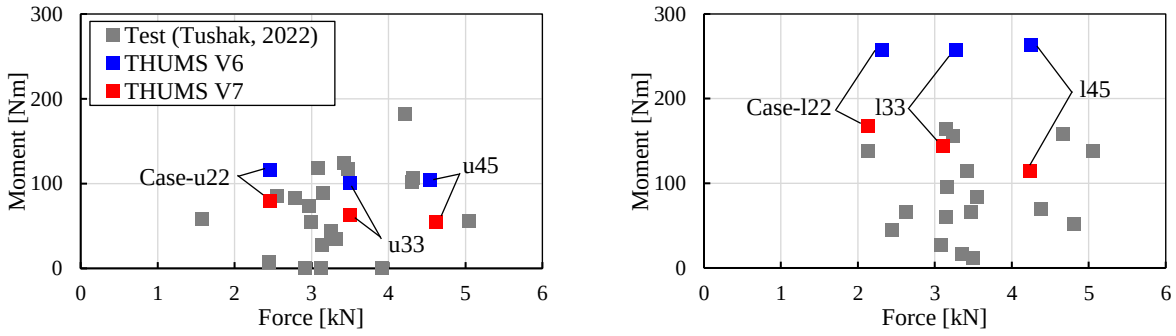


(a) Upper segment (b) Lower segment

***Figure 23. Flexional moments and compressive loads at vertebral fracture.***

**Whole-Body Validation**

**Frontal collision in forward-facing seating** Reed et al. (2019) [3] conducted a frontal impact sled test with PMHS seated in a reclining position. The seatback angle was set to 45deg. At the time of writing this manuscript, the test results at 32 kph were available in the NHTSA Database [39]. This test was used for the validation. Figure 24 illustrates the simulation model with Version 7 to reproduce the test for validation purpose. Figure 25 shows the time history waveforms of sled G pulse. The average height and weight of the three PMHS used in the test were 174 cm and 70 kg, respectively. THUMS AM50 model (179 cm, 78 kg), which was close to the subject body size, was selected for the simulation. The measured coordinate values of each part of the three PMHS were used as the reference. The initial posture of THUMS was adjusted by the following procedure. The pelvic angle was adjusted so that the angle of the line connecting hip-point and the center of the intervertebral disc between L5 and S1 became 68.4deg which was the average measured value in the tests. The spinal alignment was adjusted so that the coordinates of the head, T1, T8, T12, and L4 stayed within the range of test variation. The simulation model replicated the spring-controlled semi-rigid seat used in the PMHS test [40]. The seat pan (seat rear) angle, anti-submarine ramp (seat front) angle and spring characteristics were set to the values in the test. The relative position between the ASIS and lap belt was arranged to match the measurement values in the test.

Figure 26 compares the impact kinematics of PMHS and Version 7 in lateral view. Both PMHS and THUMS showed forward motions with the upper body bending forward and the pelvis tilting backward. In both PMHS and THUMS, the engagement between the lap belt and pelvis was maintained until the end of the impact. Figure 27 compares the trajectories of each measurement point in PMHS and THUMS. Figure 28 compares the displacement history of each part in the X and Z directions (average of three tests). For all measurement points, the trajectories of Version 7 were almost entirely within the variation range of the PMHS tests. The displacement histories for each of the THUMS sections were close to the average history of the PMHS.

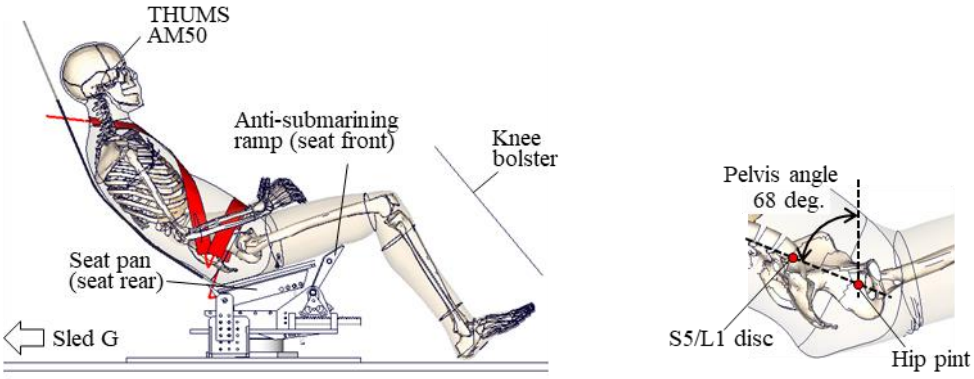


***Figure 24. Simulation model of frontal sled test in reclined posture.***

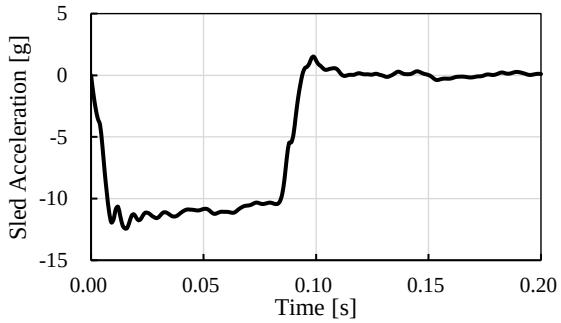


***Figure 25. Sled G pulse (delta V: 32 kph).***

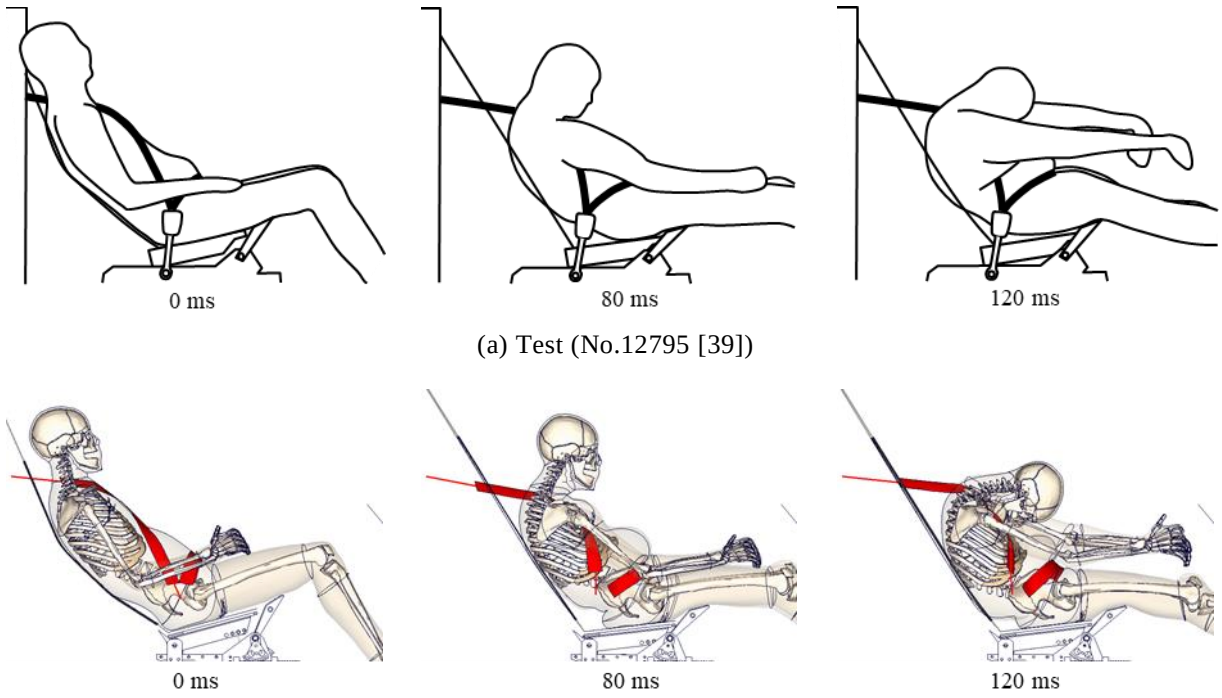


***Figure 26. Kinematics of occupant.***

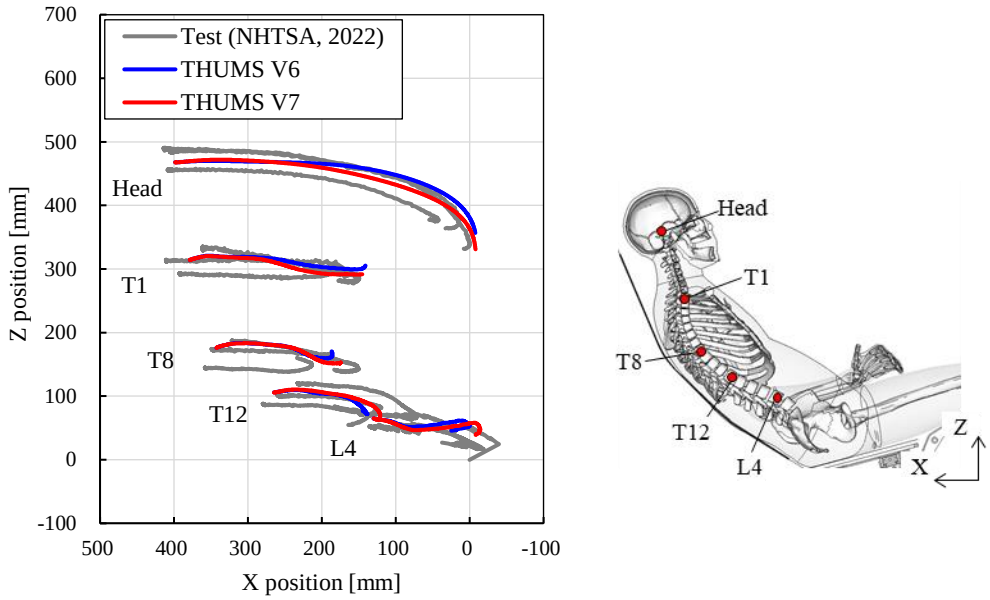


***Figure 27. Trajectories of each measurement point of occupant.***

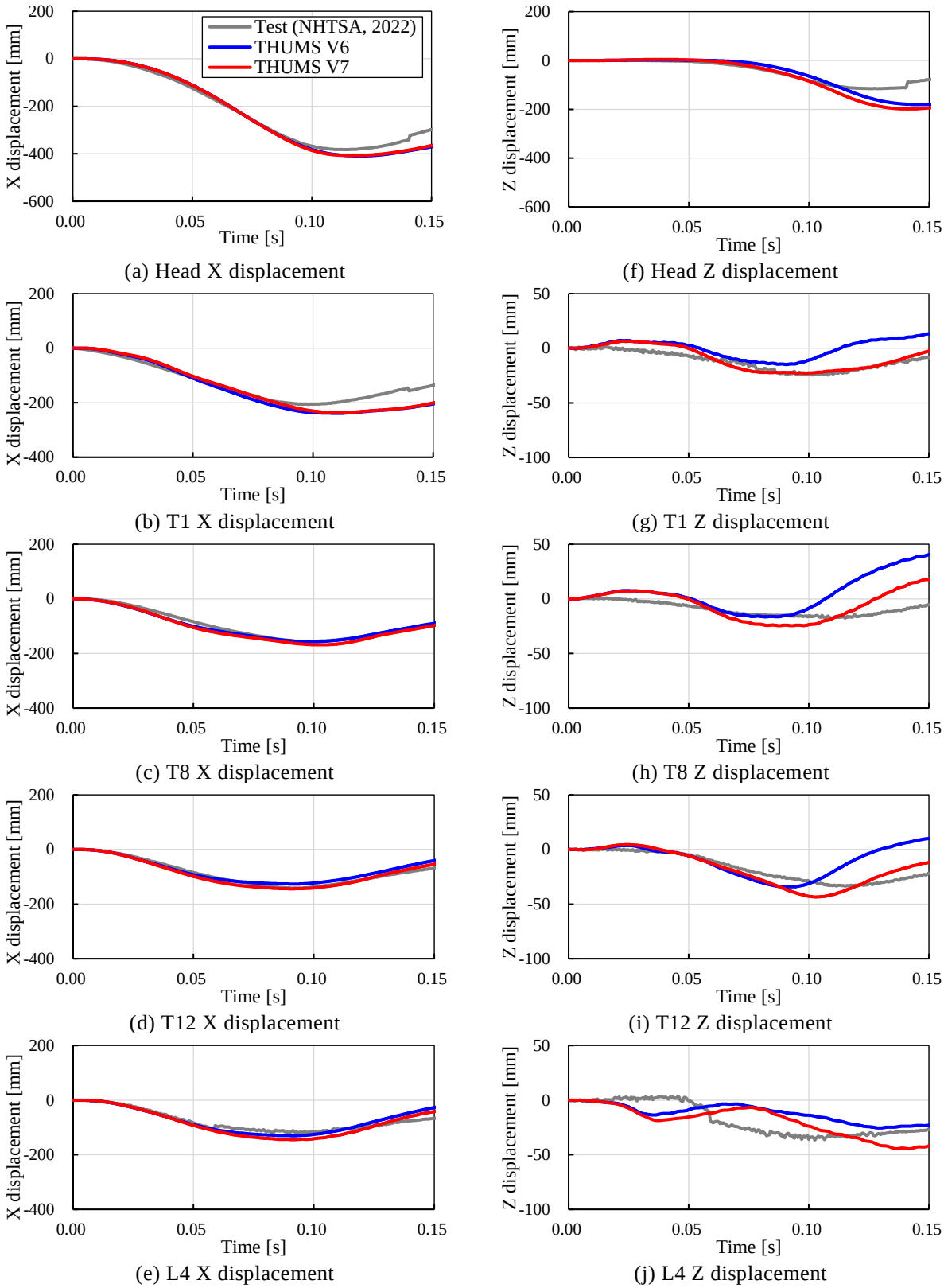


***Figure 28. Displacement time histories of each measurement point.***

The ISO rating specified in ISO/TS 18571 [41] was calculated to quantitatively evaluate the agreement of two time history curves. The closer the ISO rating value is to 1, the higher the degree of conformity. Table 9 shows the evaluation results. Regarding the Z displacements at each measurement point, the ISO rating values of Version 7 were higher than those of Version 6. As a result, the average rating value was approximately 0.1 higher in Version 7. The seat (Fr, Rr) reaction forces and seatbelt (shoulder, lap) loads for each displacement history were also close to the test load levels (Figure 29).

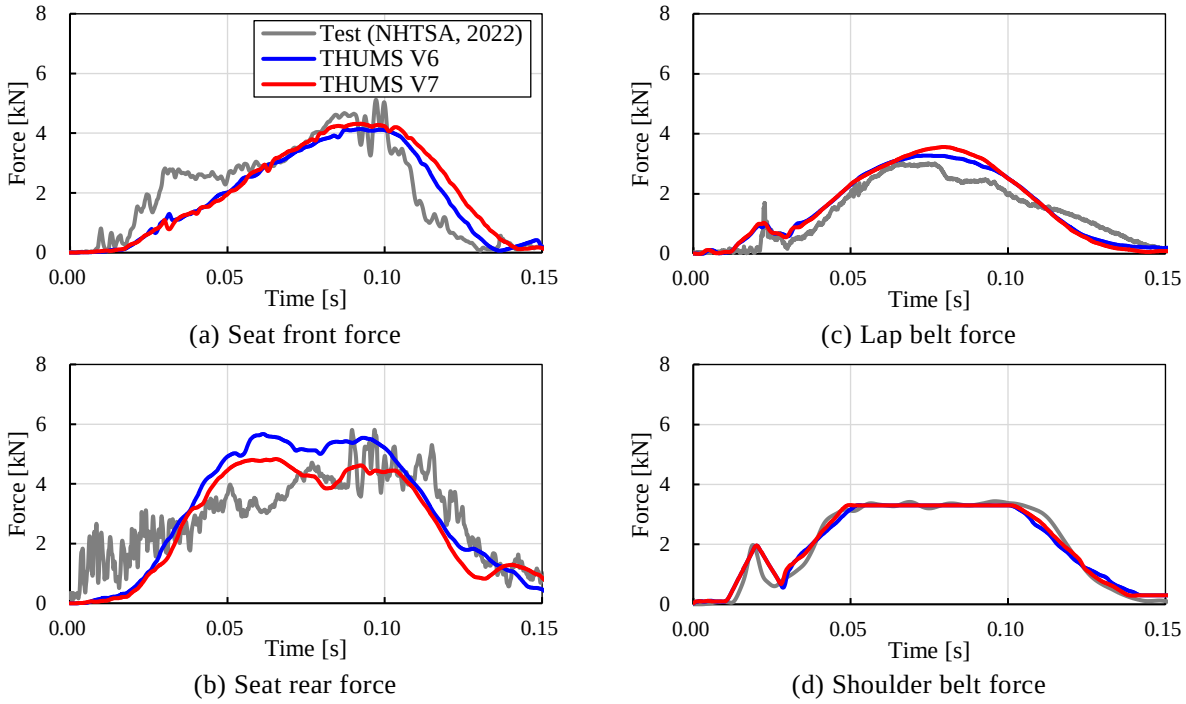


***Figure 29. Time history of seat reaction forces and belt forces.***

***Table 9.***
***Evaluated values (ISO ratings) of the match with the test curves.***

| Displacement | | THUMS V6 | | THUMS V7 | |
|---|---|---|---|---|---|
| | | ISO rating | Grade | ISO rating | Grade |
| Head | X | 0.91 | Good | 0.92 | Good |
| | Z | 0.66 | Fair | 0.66 | Fair |
| T1 | X | 0.78 | Fair | 0.78 | Fair |
| | Z | 0.28 | Poor | 0.73 | Fair |
| T8 | X | 0.94 | Excellent | 0.92 | Good |
| | Z | 0.36 | Poor | 0.42 | Poor |
| T12 | X | 0.83 | Good | 0.92 | Good |
| | Z | 0.36 | Poor | 0.70 | Fair |
| L4 | X | 0.78 | Fair | 0.79 | Fair |
| | Z | 0.29 | Poor | 0.41 | Poor |
| Average | | 0.62 | Poor | 0.73 | Fair |

## DISCUSSION

### Abdominal Organ Injuries Prediction

In the component validations, the maximum strain of the intestinal tract was calculated by simulating the abdominal loading tests with PMHS. In the test, the intestinal tract was damaged only in Case-b2. On the other hand, the maximum axial strain of the intestinal tract calculated by THUMS Version 7 was lowest in Case-b2. Figure 30 shows the abdominal deformation and strain distribution of the intestinal tract at the time of maximum intestinal strain in Case-b2 and Case-b3. In Case-b2, the displacement of the lap belt was 131 mm, which was larger than that in Case-b3 (115 mm). In Case-b2, the lap belt was tilted 30° from the horizontal and the abdominal deflection perpendicular to the body axis was 109 mm. The lap belt generated an energy of 567 J to the abdomen, which was less than 846 J in Case-b3. The fact that the maximum strain on the intestinal tract in Case-b2 was smaller than the value in Case-b3 was consistent with the energy amount relationship. Therefore, the calculated intestinal strain is considered to be reasonable. In the test of Case-b2, a water-filled balloon was inserted into the intestinal tract to measured intestinal stretch. Intestinal injury occurred at 15 locations. Nine of these occurred near the balloon and four occurred between the balloons. This suggests that the balloon affected the occurrence of intestinal injury. Of the six test cases used for simulations, intestinal injury was confirmed only in Case-b2. There is not a sufficient number of data to determine the validity of the predicted results. The mean value of the measured data [21], 37%, was assumed as the threshold for intestinal rupture. However, the standard deviation was 13%, which indicated a large variation. It is desirable to continue to accumulate damage data for validation. Probabilistic damage risk curves can be calculated from simulations. Further data accumulation and model validation are needed for the accurate prediction of mesenteric and vascular damage.

### Whole-Body Kinematics Prediction

The whole-body impact kinematics was examined in the frontal collision condition with THUMS Version 7 seated in the reclining position. Figure 27 compares the displacement history curves of key landmarks between THUMS and the PMHS. The curve obtained from Version 7 was closer to the test results than that from Version 6. Comparing the ISO rating values of the two, Version 7 upper body values for Z displacement were better than those for Version 6. Figure 31 shows the spine deformation of the mid-section at 100 ms, when the Z displacement of T1 reached its maximum. The stress distribution in the intervertebral discs and ligaments around the spine was also displayed. In Version 7, the curvature of the spine during flexion was greater than that in Version 6. The position of T1 was about 12 mm lower (Figure 31(a)). As shown in Figure 31(b), the stresses generated in the intervertebral discs and ligaments in Version 7 were lower than those in Version 6. The characteristics of the intervertebral discs and ligaments were revised in Version 7. That lowered the bending stiffness of the spine. The more flexible spine generated a larger Z-displacement at key landmarks and approached the test data. Note that test the conditions did not cause disengagement of the lap belt from the pelvis. The improvement in accuracy of submarining prediction by modifying the pelvic geometry could not be evaluated under the given condition.

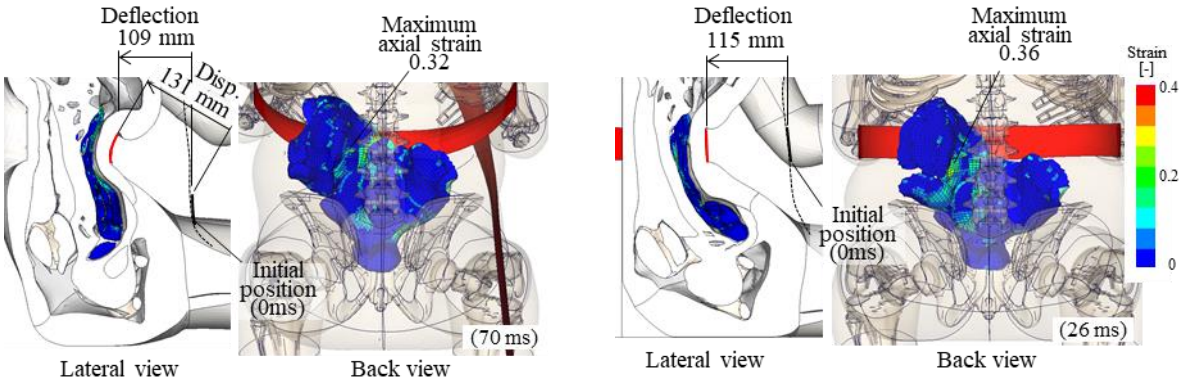


(a) Case-b2: Lap-belt, shoulder-belt (Energy: 567 J) (b) Case-b3: Lap-belt (Energy: 846 J)

***Figure 30. Comparison of abdominal deformity and intestinal tract strain.***

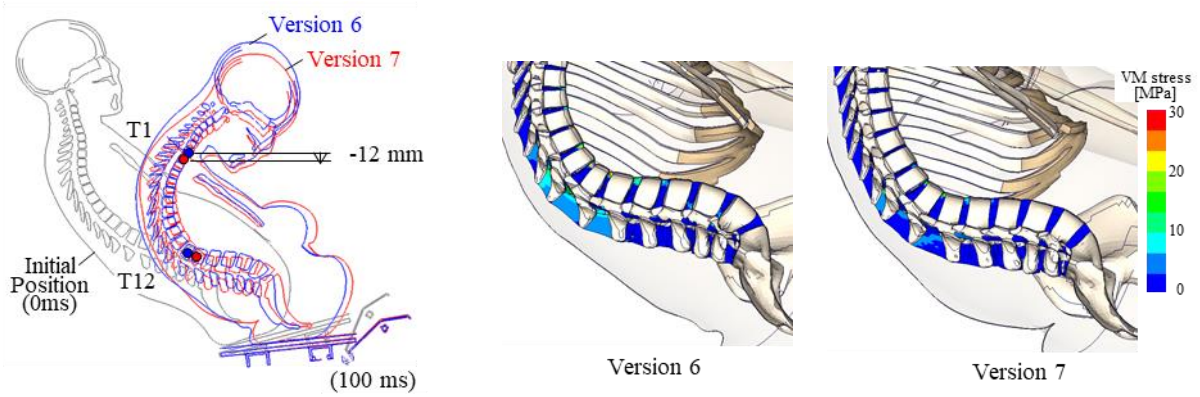


(a) Cross-sectional view in median plane (b) Stress distribution in intervertebral discs and ligaments

***Figure 31. Comparison of spine curvature.***

## LIMITATION

In a vehicle frontal collision with the occupants seated in a reclined position, there is a possibility that a large load is applied to the abdominal area including the internal organs and lumbar spine. In order to accurately predict the injury risk of the internal organs and lumbar spine, the relevant parts of THUMS have been greatly improved in Version 7. The prediction accuracy was verified under component-level loading conditions for which test data are publicly available. In the validation using the FSU, THUMS predicted vertebral fractures at loading levels close to those in the physical tests. Fracture prediction was not validated for the entire lumbar spine or the entire vertebrae. There are few published test data on damage to the intestinal tract, mesentery, and blood vessels of the small intestine. It is necessary to continue component-level verification, as well as to accumulate test data that can be used as a reference for comparison and reproducible analysis based on crash data.

The vehicle frontal collision test with the occupants seated in a reclining position, referenced in this report, was conducted under a moderate speed (ΔV: 32 kph). The lap belt was well engaged with the pelvis during the test. At a high speed such as 56 kph, it is likely that the occupant moves further forward and the lap belt engagement could be lost depending on the conditions. The pelvis dimensions and the soft tissue thickness around the abdomen may affect the engagement during a collision. Future studies should include the test conditions in which lap belt disengagement could occur.

## CONCLUSIONS

This paper describes the development status of the THUMS Version 7. The objectives were first to simulate impact kinematics of an occupant seated in a reclined position during a frontal vehicle collision, and second to accurately predict injuries of the internal organs and lumbar spine. For accurate simulation of the interaction between the pelvis and lap belt, the pelvis geometry was modified to come close to the average size of each body type (AF05, AM50, AM95). The material properties of the skin and adipose tissue of the anterior pelvis were greatly improved in order to better represent those of actual human tissue. The intestinal tract and mesentery structures of the small intestine were precisely represented, and material constitutive laws were introduced to account for anisotropy. For the lumbar spine, the material properties of the intervertebral discs and ligaments were revised, and the realistic distribution of cortical bone thickness of the vertebral bodies was reproduced. The mechanical properties of the abdomen and lumbar spine were validated by comparison with component-level test results. The abdominal load response of the Version 7 when loaded with impactors and belts was found to be similar to the test results. The validity of the mechanical response of the lumbar spine when loaded in compression, shear, and bending was also examined. Comparisons were made with the available test data such that Version 7 reproduced the kinematics of an occupant seated in a reclining position during a frontal collision close to those of the PMHS.

## REFERENCES


[1] Jorlöv, S., Bohman, K., Larsson, A. 2017. "Seating Positions and Activities in Highly Automated Cars - A Qualitative Study of Future Automated Driving Scenarios." IRCOBI Conference, Antwerp, Belgium

[2] Östling, M., Larsson, A. 2019. "Occupant Activities and Sitting Positions in Automated Vehicles in China and Sweden." 26th International Technical Conference on the Enhanced Safety of Vehicles (ESV), 19-0083, Eindhoven, Netherlands

[3] Reed, M. P., Zaseck, L., Hu, J. 2019. "Automated Vehicle Occupant Kinematics - Phase I :Task Implementation Plan." University of Michigan Transportation Research Institute

[4] Kang, Y.-S., Stammen, J., Ramachandra, R., Agnew, A. M., Hagedorn, A., Thomas, C., Kwon, H. J., Moorhouse, K., Bolte IV., J. H. 2020. "Biomechanial Responses and Injury Assessment of Post Mortem Human Subjects in Various Rear-facing Seating Configurations." Stapp Car Crash Journal, Vol. 64, 155-212

[5] Richardson, R., Donlon, J.-P., Jayathirtha, M., Forman, J. L., Shaw, G., Gepner, B., Kerrigan, J. R. 2020. "Kinematic and Injury Response of Reclined PMHS in Frontal Impacts" Stapp Car Crash Journal, Vol. 64, 83-153

[6] NHTSA, 2017. "Automated Driving Systems 2.0 - A Vision for Safety." Internet: [https://www.nhtsa.gov/sites/nhtsa.gov/files/documents/13069a-ads2.0_090617_v9a_tag.pdf], Data Accessed November 3, 2022

[7] Boyle, K. J., Reed, M. P., Zaseck, L. W., Hu, J. 2019. "A Human Modelling Study on Occupant Kinematics in Highly Reclined Seats during Frontal Crashes." IRCOBI Conference, Florence, Italy

[8] Lin, H., Gepner, B., Wu, T., Forman, J., Panzer, M. 2018. "Effect of Seatback Recline on Occupant Model Response in Frontal Crashes." IRCOBI Conference, Athens, Greece

[9] Draper, D., Huf, A., Wernicke, P., Peldschus, S. 2019. "The Influence of Rellined Seating Positions on Lumbar Spine Kinematics and Loading in Frontal Impact Scenarios." 26th ESV Conference, 19-0062, Eindhoven, Netherlands

[10] Gepner, B.D., Draper, D., Mroz, K., Richardson, R., Ostling, M., Pipkorn, B., Forman, J. L., Kerrigan, J. R. 2019. "Comparison of Human Body Models in Frontal Crashes with Reclined Seatback" IRCOBI Conference, Florence, Italy

[11] Mroz, K., Östling, M., Richardson, R., Kerrigan, J., Forman, J., Gepner, B., Lubbe, N., Pipkorn, B. 2020. "Effect of Seat and Seat Belt Characteristics on the Lumbar Spine and Pelvis Loading of the SAFER Human Body Model in Reclined Postures", IRCOBI Conference, Munich, Germany

[12] Shigeta, K., Kitagawa, Y., Yasuki, T. 2009. "Development of Next Generation Human Body FE Model Capable of Organ Injury Prediction." 21st ESV Conference, 09-0111, Stuttgart, Germany

[13] Iwamoto, M., Nakahira, Y., Kimpara, H. 2015. "Development and Validation of the Total HUman Model for Safety (THUMS) Toward Further Understanding of Occupant Injury Mechanisms in Precrash and During Crash." Traffic Injury Prevention, 16 sup1, S36–S48

[14] Iwamoto, M., Nakahira, Y., Tamura, A., Kimpara, H., Watanabe, I., Miki, K. 2007. "Development of Advanced Human Models in THUMS." 6th European LS-DYNA Users' Conference, Gothenburg, Sweden

[15] Kato, D., Nakahira, Y., Atsumi, N., Iwamoto, M. 2018. "Development of Human-Body Model THUMS Version 6 Containing Muscle Controllers and Application to Injury Analysis in Frontal Collision after Brake Deceleration." IRCOBI Conference, Athens, Greece

[16] Hwang, E., Hallman, J., Klein, K., Rupp, J., Reed, M. P., Hu, J. 2016. "Rapid Development of Diverse Human Body Models for Crash Simulations through Mesh Morphing." SAE 2016-01-1491

[17] University of Michigan Transportation Research Institute (UMTRI), "Human Shapes: Realistic Human Body Shape Modeler Based on Real Data" Internet: [http://humanshape.org/], Data Accessed November 3, 2022

[18] Annaidh, A. N., Bruyere, K., Destrade, M., Gilchrist, M. D., Ottenio, M. 2012. "Characterization of the Anisotropic Mechanical Properties of Excised Human Skin." Journal of the Mechanical Behavior of Biomedical Materials, 5, 139-148

[19] Sun, Z., Lee, S.-H., Gepner, B. D., Rigby, J., Hallman, J. J., Kerrigan, J. R. 2021. "Comparison of Porcine and Human Adipose Tissue Loading Responses under Dynamic Compression and Shear: A Pilot Study." Journal of the Mechanical Behavior of Biomedical Materials, 113, 104112

[20] Nakahira, Y., Watanabe, I., Iwamoto, M. 2019. "Investigation of Small Intestine and Mesentery Modeling Methods to Analyze Traumatic Abdominal Injury." JSAE 20196202

[21] Egorov, V. I., Schastlivtsev, I. V., Prut, E. V., Baranov, A. O., Turusov, R. A. 2002. "Mechanical Properties of the Human Gastrointestinal Tract" Journal of Biomechanics, 35, 1417–1425

[22] Inoue,T. 1957. "Experimental Studies on Physical Strength of Gastrointestinal Serous Membranes." Medical Journal of Kobe University, Vol. 11, No. 3, 420-435
[23] Yamada, H., Evans, F.G. (Ed.) 1970. "Strength of Biological Materials" Williams & Wilkins, USA
[24] Kemper, A., McNally, C., Manoogian, S., McNeely, D., Duma, S. 2013. "Stiffness Properties of Human Lumbar Intervertebral Discs in Compression and the Influence of Strain Rate." SAE 07-0471, 127-133
[25] Lourenço, C., Claro, J. C. P. 2015. "Biomechanical Experimental Data Curation: An Example for Main Lumbar Spine Ligaments Characterization for a MBS Spine Model." Mechanisms and Machine Science, ISSN 2211-0984, Vol. 24
[26] Picazo, M. L., Baro, A. M., Barquero, L. M. D. R., Gregorio, S. D., Martelli, Y., Romera, J., Steghöfer, M., Ballester, M. A. G., Humbert, L. 2018. "3-D Subject-Specific Shape and Density Estimation of the Lumbar Spine from a Single Anteroposterior DXA Image Including Assessment of Cortical and Trabecular Bone" IEEE Transactions Medical Imaging, 37(12), 2651-2662
[27] Zhao, F.-D., Pollintine, P., Hole, B. D., Adams, M. A., Dolan, P. 2009. "Vertebral Fractures Usually Affect the Cranial Endplate Because It Is Thinner and Supported by Less-dense Trabecular Bone." Bone, 44(2), 372–379
[28] Ritzel, H., Amling, M., Pösl, M., Hahn, M., Delling, G. 1997. "The Thickness of Human Vertebral Cortical Bone and Its Changes in Aging and Osteoporosis: A Histomorphometric Analysis of the Complete Spinal Column from Thirty-Seven Autopsy Specimens." Journal of Bone and Mineral Research, Vo. 12, No. 1
[29] Kerrigan, J. 2020. "Experiments to Address Limitations in Biofidelity of Human Body Models for Autonomous Vehicles" Government/Industry Meeting, Washington, USA
[30] Cavanaugh, J. M., Nyquist, G. W., Goldberg, S. J., King, A. I. 1986. "Lower Abdominal Tolerance and Response" 30th Stapp Car Crash Conference, SAE 861878, 41-63
[31] Nusholtz, G. S., Kaiker, P. S., Lehman, R. J. 1988. "Steering System Abdominal Impact Trauma" UMTRI-88-19, Michigan, USA
[32] Hardy, W. N., Schneider, L. W., Rouhana, S. W. 2001. "Abdominal Impact Response to Rigid-Bar, Seatbelt, and Airbag Loading." Stapp Car Crash Journal, Vol. 45
[33] Howes, M. K., Hardy, W. N. 2015. "Evaluation of the Kinematic Responses and Potential Injury Mechanisms of the Jejunum during Seatbelt Loading" Stapp Car Crash Journal, Vol. 59, 225-267
[34] Foster, C. D., Hardy, W. N., Yang, K. H., King A. I. 2006. "High-Speed Seatbelt Pretensioner Loading of the Abdomen." Stapp Car Crash Journal, Vol. 50, 27-51
[35] Arun, M. W. J., Hadagali, P., Driesslein, K., Curry, W., Yoganandan, N., Pintar, F. A. 2017. "Biomechanics of Lumbar Motion-Segments in Dynamic Compression." Stapp Car Crash Journal, Vol. 61, 1-25
[36] Belwadi, A., Yang, K. H. 2008. "Response of the Cadaveric Lumbar Spine to Flexion, with and without Anterior Shear Displacement." IRCOBI Conference, Bern, Switzerland
[37] Chastain, K. L. 2021. "Characterization of the Mechanical Response of the Lumbar Spine: The Effect of a Compressive Axial Load." Master's Thesis for the University of Virginia
[38] Tushak, S. K., Donlon, J. P., Gepner, S. D., Chebbi, A., Pipkorn, B., Hallman, J. J., Forman. J. L., Kerrigan, J. R. 2022. "Failure Tolerance of the Human Lumbar Spine in Dynamic Combined Compression and Flexion Loading." Journal of Biomechanics, 135, 111051
[39] NHTSA, 2022. "Biomechanics Test Database" Internet: [https://www.nhtsa.gov/research-data/research-testing-databases#/biomechanics], Data Accessed September 19, 2022
[40] Uriot, J., Potier, P., Baudrit, P., Trosseille, X., Petit, P., Richard, O., Compigne, S., Masuda, M., Douard, R. 2015. "Reference PMHS Sled Tests to Assess Submarining." Stapp Car Crash Journal, Vol. 59
[41] ISO/TS 18571, 2014. "Road vehicles - Objective Rating Metric for Non-ambiguous Signals." International Organization for Standardization, Geneva, Switzerland
[42] Gordon, C. C., Blackwell, C. L., Bradtmiller, B., Parham, J. L., Barrientos, P., Paquette, S. P., Corner, B. D., Carson, J. M., Venezia, J. C., Rockwell, B. M., Mucher, M., Kristensen, S. 2014. "2012 Anthropometric Survey of U.S. Army Personnel: Methods and Summary Statistics." U.S. Army Natick Soldier Research, Development and Engineering Center, Natick, Massachusetts, USA
[43] Mohr, M., Abrams, E., Engel, C., Long, W. B., Bottlang, M. 2007."Geometry of Human Ribs Pertinent to Orthopedic Chest-Wall Reconstruction." Journal of Biomechanics, 40, 1310-1317
[44] Charpail, E., Trosseille, X., Petit P., Laporte, S., Lavaste, F., Vallancien, G. 2005. "Characterization of PMHS Ribs: A New Test Methodology." Stapp Car Crash Journal, Vol. 49, 183-198
[45] Netter, F. H. 2007. "Netter Atlas of Human Anatomy 4th Ed." Elsevier

## APPENDIX

### Other Modifications and Validations

In addition to the model modifications of the abdomen and lumbar region, another four items were updated in THUMS Version 7 as shown in Table 1, Body Region - Others. The details of the updates are described below.

**Head Model** The head sizes were revised. The mean measured head dimensions [42] and THUMS dimensions for each body type (AF05, AM50, AM95) are shown in Table A-1. The head dimensions were adjusted to match the average size.

**Rib Model** Version 6 assumed uniform cortical bone thickness in all ribs. Version 7 considered the realistic distribution of cortical bone thickness [43] for the ribs (Figure 8). The fracture loads and deflection rates of the ribs (AM50, 4th rib) under bending loading that became closer to the test results [44] (Figure A-1).

***Table A-1.***
***Head geometry.***

| | AF05 | | | AM50 | | |
|---|---|---|---|---|---|---|
| | Measurement (Gordon, 2014) | THUMS V6 | THUMS V7 | Measurement (Gordon, 2014) | THUMS V6 | THUMS V7 |
| Breadth [mm] | 140 | 142 (+ 2) | 140 ( 0) | 154 | 165 (+11) | 154 ( 0) |
| Height [mm] | 208 | 225 (+17) | 208 ( 0) | 238 | 262 (+24) | 238 ( 0) |
| Length [mm] | 178 | 183 (+ 5) | 178 ( 0) | 200 | 212 (+12) | 200 ( 0) |
| Weight [kg] | - | 3.7 | 3.4 | - | 5.4 | 4.6 |

| | AM95 | | |
|---|---|---|---|
| | Measurement (Gordon, 2014) | THUMS V6 | THUMS V7 |
| Breadth [mm] | 163 | 165 (+ 2) | 163 ( 0) |
| Height [mm] | 251 | 262 (+11) | 251 ( 0) |
| Length [mm] | 211 | 212 (+ 1) | 211 ( 0) |
| Weight [kg] | - | 5.4 | 5.3 |

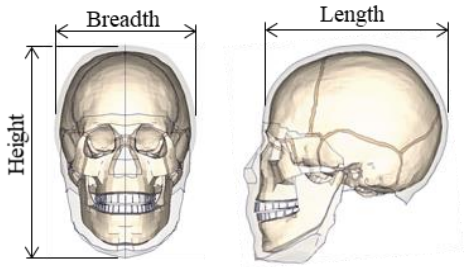


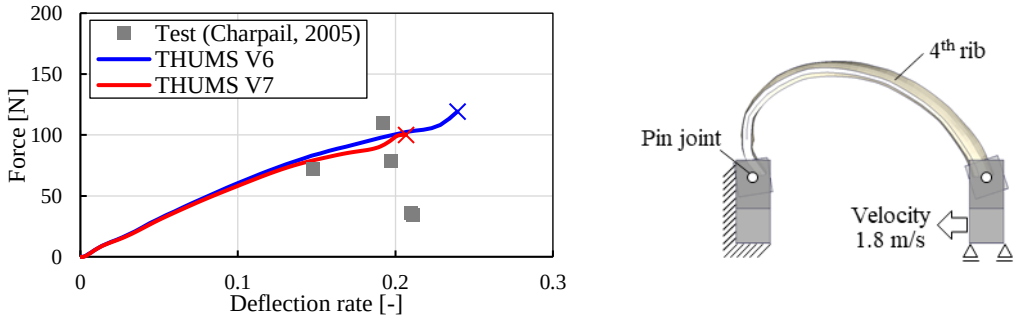


***Figure A-1. Force vs. deflection rate curve during rib bending***

**Heart Model** Version 7 more accurately represents the anatomical structure and characteristics of the heart. Figure A-2 shows the heart models of Version 6 and Version 7. The heart model of Version 6 was modeled as a single homogeneous structure. In Version 7, the septal wall, the connections with the great vessels, and the blood inside were separately represented [45]. The myocardium was modeled using hexa-elements with three or more elements in the thickness direction, and large blood vessels such as the aorta and vena cava were modeled using a single hexa-solid element. The material properties [23] were assumed to be hyperelastic. The blood was filled inside the heart and blood vessels with tetra-solid elements. The material properties of the blood were assigned with Elastic fluid model. The load response characteristics of the heart examined by applying a compressive load on a rigid table. The simulation result was found to be close to the test result (Figure A-3).

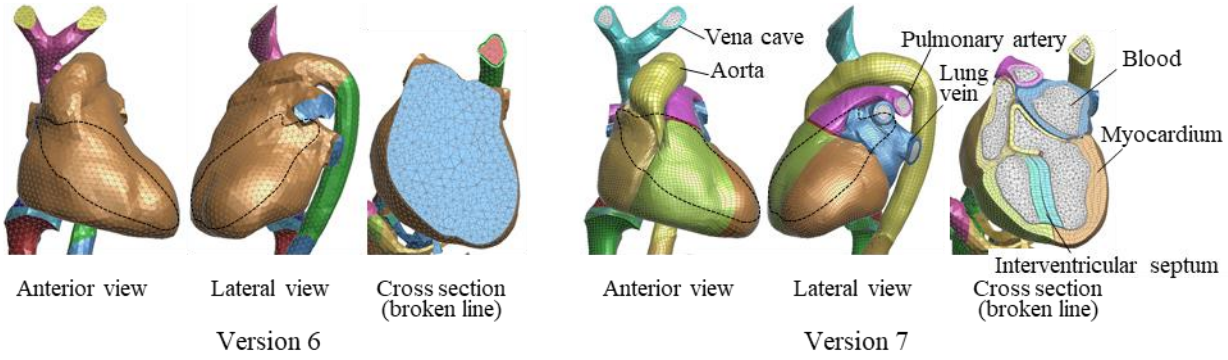


***Figure A-2. Heart model.***

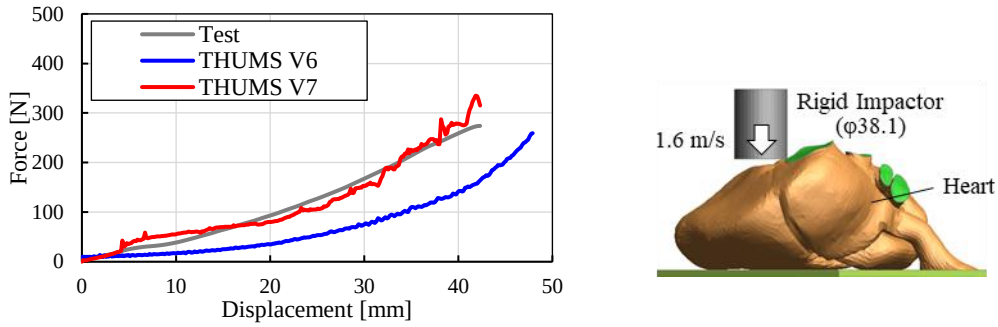


***Figure A-3. Force vs. deflection rate curve in heart compression***

**Long Bone Model** In Version 6, the inside part of the long bones (femur, tibia, fibula, and humerus) was assumed as cancellous bone. In Version 7, the internal marrow section was added to mimic the actual bony structure [45] (Figure A-4). The load-displacement characteristics of the femur in three-point bending are shown in Figure A-5. The load-displacement characteristics of the Version 7 femur were close to the test results [23].


***Figure A-4. Long bone model (Femur).***

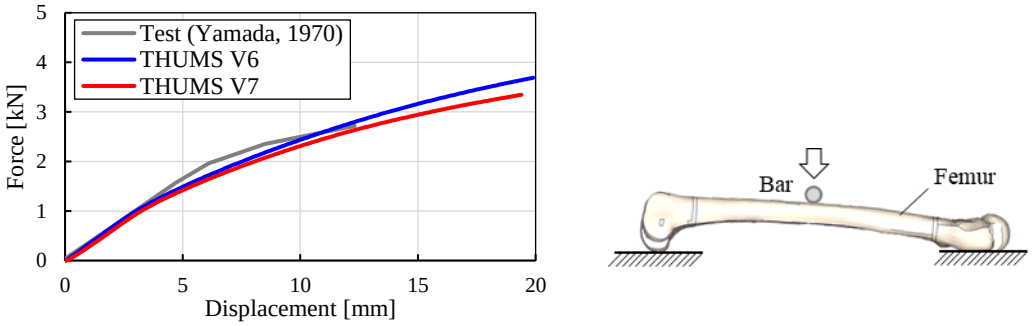


***Figure A-5. Force vs. deflection rate curve during femur 3-point bending***